Design and analysis of kinematically redundant planar parallel manipulator for isotropic stiffness condition

By

Mr. Divekar Aniket Ashok

Department of Mechanical Engineering
National Institute of technology, Rourkela
Rourkela - 769 008, Odisha, INDIA
2012-2014

Design and analysis of kinematically redundant planar parallel manipulator for isotropic stiffness condition

A thesis submitted in partial fulfillment of the

requirements for the degree of

Master of Technology
in
Machine Design and Analysis
by

Mr. Divekar Aniket Ashok
(Roll No: 212 ME 1274)

Under the guidance of
Dr. (Prof.) J. Srinivas

Department of Mechanical Engineering
National Institute of technology, Rourkela
Rourkela - 769 008, Odisha, INDIA
2012-2014

Department of Mechanical Engineering
National Institute of Technology, Rourkela

C E R T I F I C A T E

This is to certify that the thesis entitled, ***"Design and analysis of kinematically redundant planar parallel manipulator for isotropic stiffness condition"*** *by* ***Mr. Divekar Aniket Ashok****,submitted to the National Institute of Technology, Rourkela for the award of Master of Technology in* ***Mechanical Engineering*** *with the specialization of "****Machine Design & Analysis****", is a record of bonafide research work carried out by him in the* ***Department of Mechanical Engineering,*** *under my supervision and guidance. I believe that this thesis fulfills part of the requirements for the award of the degree of Master of Technology. The results embodied in this thesis have not been submitted for the award of any other degree elsewhere.*

Dr. (Prof.) J. Srinivas
Dept. of Mechanical Engineering
National Institute of Technology
Rourkela-769008, Odisha,
INDIA

Place:
Date:

ACKNOWLEDGEMENT

First and foremost, I wish to express my sense of gratitude and indebtedness to my supervisor Prof. J. Srinivas for their inspiring guidance, encouragement, and untiring efforts throughout the course of this work. Their timely help, constructive criticism and painstaking efforts made it possible to present the work contained in this thesis.

I express my gratitude to the professors of my specializations for their advice and care during my tenure. I am also very much obliged to the Head of Department of Mechanical Engineering Prof. K. P. Maity, NIT Rourkela for providing all the possible facilities towards this work. Also thanks to the other faculty members in the department.

Specially, I extend my deep sense of indebtedness and gratitude to my colleagues, Mr. Shivprasad Baad, Virendra Mathpati and Mahesh Pol and my sinior, Ms. Varlakshmi mam for their enjoyable and helpful company. After the completion of this Thesis, I experience a feeling of achievement and satisfaction. Looking into the past I realize how impossible it was for me to succeed on my own. I wish to express my deep gratitude to all those who extended their helping hands towards me in various ways during my tenure at NIT Rourkela.

I am especially indebted to my parents for their love, sacrifice and support. They are my first teachers after I came to this world and have set great examples for me about how to live, study and work.

Divekar Aniket Ashok

Rourkela, June 2014

ABSTRACT

Parallel manipulators are a form of closed loop linkages and have a wide range of applications e.g. surgical robots, flight simulators, pointing devices etc. Parallel mechanisms have many advantages over serial manipulator. Higher accuracy, stiffness and increased payload capacity are the characteristics of parallel manipulator. In spite of many advantages, they have limited workspace and more singularity regions. So, redundant architectures have become popular. However, redundancy leads to infinite solutions for inverse kinematic problem. The current work addresses this issue of resolving the redundancy of kinematically redundant planar parallel manipulators using optimization based approach. First the conventional non-redundant 3-RPR planar parallel manipulator is presented. Afterwards the kinematically redundant counterpart 3-PRPR is discussed and actuation redundant 4-RPR has been touched upon briefly. Computer simulations have been performed for the kinematic issues using MATLAB programme . The workspace of redundant and non-redundant parallel manipulators have been obtained. The generalized stiffness matrix has been derived based upon the Jacobian model and the principle of duality between kinematics and statics. A stiffness index has been formulated and the isotropy of stiffness index is used as the criterion for resolving redundancy. A novel spiral optimization metaheuristics has been used to achieve the isotropic stiffness within the selected workshape and the results are compared against particle swarm optimization. The results obtained from the novel Spiral optimization are found to be more effective and closer to the objective function as compared to the particle swarm optimization. Optimum redundant parameters are obtained as a result of the analysis. A wooden skeletal prototype has also been fabricated to enhance the understanding of the mechanism workability.

INDEX

Nomenclature

M	Mobility of kinematic chain
f	Degree of freedom of kinematic pair or chain
t_{ij}	Displacement of j^{th} joint of i^{th} limb
$\hat{n}_{ij}$	Direction vector of the displacement of j^{th} joint in i^{th} limb
J	The Jacobian matrix
f	The joint force vector
F	The applied or cartesian force vector
K_j	Diagonal stiffness matrix for actuators
K	The stiffness matrix for manipulator
S	Stiffness index
r	Spiral radius
¤	Spiral angle
R^m	M-dimensional rotation matrix
w	Weight factor in particle swarm optimization
c_i	Social weight factors in particle swarm optimization

LIST OF FIGURES

LIST OF TABLES

Chapter-1

Introduction

Parallel mechanisms are found recently in many applications including machine tools, robots and simulation platforms etc. Unlike serial manipulator used in most industrial robots, here, all the joint motors are located at ground level and a sort of stiffness improvising mechanism is provided in the structure. Thus, essentially, a parallel linkage provides advantages such as improved stiffness to weight ratio and more accurate path following capabilities. They are finding several applications in micro and nano level devices. Basic parallel linkage is a 6-DOF stewart-Guff spatial platform studied by several researchers. More recently, planar parallel mechanisms are being employed in several application areas. Most common, planar parallel linkages are 3-RRR, 3-RPR and 3-PRR linkages. Here, the underscore denotes the actuator location in the mechanism; for example 3-RRR indicates that the mechanism has 3 chains each having three revolute joints with first revolute joint as actuation joint. All these mechanisms drive a platform in a plane motion (3 degrees of freedom) allowing the platform point (cutting tool) to move according to a desired path/trajectory. Main disadvantages of these linkages are their relatively small workspace and huge singularities within the workspaces. At singularities, the mechanism either loses (forward) or gains (inverse) a degree of freedom and cannot perform the action as per the instructions. Such mechanisms with sufficient DOF for a specific end-effector task may not have the ability to achieve alternative paths when attempting a task due to their uniqueness of solution. In order to alleviate these problems, several efforts are made in literature. An important attempt in this direction is to provide

redundancy in the mechanism. Redundancy refers to the adding additional actuator to achieve the same three degrees of freedom at the platform point (end-effector). Additional actuators may avoid singular postures and improvise dexterity in path planning just like a serial human hand mechanism. But, the mechanism becomes more complex leading to several possible joint solutions to achieve a desired task. Resolving the complexity in kinematics and dynamics of mechanisms is one of the important issues in redundant parallel mechanisms.

1.1 Redundant Parallel Manipulators

There are mainly two different types of redundancy in parallel manipulators: (a) kinematic redundancy and (b) actuation redundancy. A parallel manipulator is said to be kinematically redundant when its mobility is more than the degrees of freedom at the moving platform. We often use this type of redundancy for enhancing the workspace. Fig.1.1 shows an example of kinematically redundant manipulators.

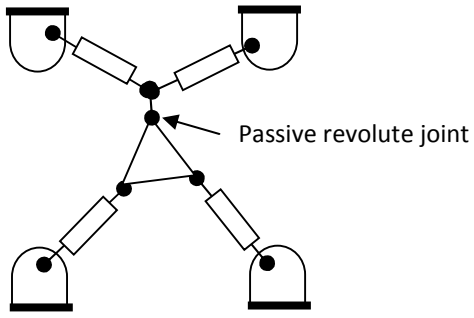

Fig.1.1 Kinematically redundant

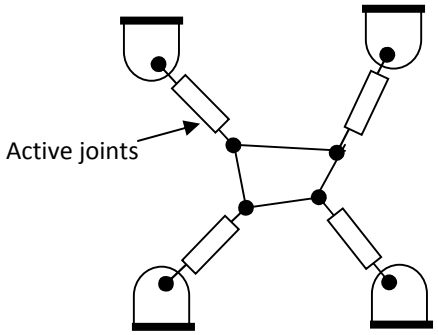

Fig.1.2 Redundantly actuated

The mobility or degrees of freedom M is given by $M=\lambda(L-J-1)+\sum f_j$, $j=1,2,\ldots J$; with λ as motion parameter (3 in case of planar and 6 in case of spatial), L and J as total number of links and joints respectively and f_j as the degree of freedom at each joint in the linkage. In

case of kinematically redundant manipulators, mobility M is greater than λ and is equal to the number of actuators used in the mechanism.

On the other hand, a parallel manipulator is redundantly actuated when the number of actuators is greater than the mobility of the mechanism (Fig.1.2). Redundant actuation does not change mobility of mechanism M, but increases only the number of actuators. That is mobility M=λ and the number of actuators used in linkage are greater than this mobility M.

Redundant actuation in parallel manipulator can be implemented by the following approaches. The first one is to actuate some of the passive joints within the branches of the parallel manipulator. The second one is to add some additional branches beyond the minimum necessary to actuate the parallel manipulator. The last one can be the hybrid of the above two approaches.

1.2 Liteature review

Several earlier works explained various insights of parallel redundant manipulators. These can be grouped under different headings like: workspace, singularities, dynamics and control and so on. Here, a brief literature relating to redundant parallel manipulators is described.

A systematic classification of redundancies in parallel manipulators was proposed by Lee and Kim [1] and Marlet [2]. Accordingly, there are three types of redundancies, Type I, Type II and Type III that are achieved by adding additional joint to existing limbs, replacing passive joints in current limbs with active ones and adding additional limbs. Redundancy can provide practical advantages to industrial manipulators.

Redundantly actuated linkages

Abundant literature is available on redundantly actuated manipulators since early 2000. Firmani and Podhorodeski [3] presented a study of the effect of redundant actuators on the existence of force-unconstrained configurations of planar parallel layout of joints. Successively, a methodology of using scaling factors to determine the force capabilities of redundantly-actuated parallel manipulators was also presented [4]. Wu et al. [5] described dynamics and control of a three degree of freedom parallel kinematic machine tool with actuation redundancy. Muller and Hufnagel [6] presented computed torque control scheme in redundant coordinates to control redundantly actuated parallel kinematic machine. A 2 degree of freedom model was used to illustrate methodology. More recently, an idea of optimizing antagonistic stiffness for redundantly actuated mechanisms for resolving redundancy was proposed by Shin et al.[7].

Kinematically redundant manipulators

Mohamed and Gosselin [8] addressed the issue of kinematic redundancy using 3-RRR mechanism. The requirement may be improvement of dexterity or stiffness etc. This is an important observation, since it helps identify the utility of the redundant mechanism. Wang and Gosselin [9] carried out analysis and design of parallel manipulator both planar as well as spatial using kinematic redundancy. A significant reduction in the singularity region was obtained via addition of the redundancy.

Ebrahimi [10] dealt with analysis of four different types of kinematically redundant planar parallel manipulators. They compared the dexterous workspace for the kinematically redundant planar parallel manipulators with conventional non-redundant planar parallel case. Later-on, Ebrahimi *et al*.[11] presented a novel redundant 3-PRRR

architecture, considering its advantages over the non-redundant one. The same authors [12] proposed actuation schemes for 3-RRR and 3-PRRR using optimization procedures. The problem of finding a valid actuation scheme for parallel manipulators is one of the least explored. Two techniques were presented, first one based upon the condition number of the Jacobian matrix and the second scheme was derived from scaled in-circle radius method. It was shown that the solutions obtained from scaled incircle radius method provide better manipulability. Ebrahimi et al. also [13] conducted the path planning for 3-RPRR kinematically redundant planar parallel manipulator. The dexterous workspace and the actuation scheme for 3-RPRR were obtained using an index of closeness to singularity and condition number. Different actuation schemes were compared using manipulability and results indicated that kinematically redundant 3-RPRR is advantageous over 3-PRR.

Cha et al. [14-15] dealt with redundancy resolution problem by considering singularity avoidance using 3-RRR mechanism and to found out the permissible limits of the kinematically redundant active base sliders in order to avoid singularities along a specified trajectory.

Chen et al. [16] dealt with improving the positional accuracy of parallel manipulator using kinematic redundancy. With the kinematically redundant variables, optimum configurations were selected for which the error transmission is least and output errors were optimized instead of being determined.

Kortlarski et al. [17] proved the utility of kinematic redundancy to increase the useable workspace of parallel manipulator with the help of 3-(P)RRR and 3-(P)RPR .

The workspace was obtained using an interval based method for singularity avoidance along a specified trajectory.

Kotlarski et al. [18] also proposed five different strategy for resolving kinematic redundancy. The position of redundant joints was formulated in terms of optimal values of maximal homogenized pose errors of the end effector. Further it was proven that classical continuous optimization techniques resulted in same performance variables that could be obtained by discrete optimization techniques.

Zarkandi [19] carried out singularity analysis on a 3-PRRR kinematically redundant manipulator. Weihmann *et al*. [20] carried-out optimization based computation of the force capabilities of a 3-RPRR manipulator without considering the trajectory. Ruggius and Carretero [21] evaluated the kinematic performance of 3-PRPR planar parallel manipulator. Jacobian and workspace analysis was conducted. The results indicated improved performance in comparision to 3-RPR conventional manipulator.

Gallant et al. [22] proposed a geometrical procedure to determine the dexterous workspace of n-RRRR and n-RRPR kinematically redundant planar parallel manipulators. The workspace of the kinematically redundant manipulator was developed from the intersection of the kinematic sub-chains forming each limb and Gauss divergence theorem was applied to calculate the dexterous workspace area. It was shown that for kinematically redundant RRRR and RRPR limbs workspaces are dependent on the type of the non-redundant part and the dimensions of the redundant linkage.

Thanh et al. [23] dealt with modelling and dynamics identification of kinematically redundant parallel robots. A set of minimal dynamic parameters were

obtained from lagrangian equations using coordinate partitioning method. The direct search technique was used for optimization of dynamic parameters.

More recently, Boudreau and Nokleby [24] proposed a solution to the problem of redundancy resolution of the redundant parallel manipulator following a desired trajectory by optimizing the joint torques. The base architecture for the work was the conventional non-redundant 3-RPR planar parallel manipulator.

Redundancy resolution to obtain the kinematic solution of a parallel manipulator is thus based on the application considered. For example, in load carrying applications like machining, one has to account stiffness maximization, while in pick-and-place applications as in printed circuit board assemblies, one has to account dexterity and singularities as criterion.

1.3 Objectives and Scope

In kinematics of redundant parallel robots, inverse kinematics results in multiple solutions for a given pose. So, one has to consider redundancy-resolution issues, which should account joint physical limits as well as environmental factors. The redundancy-resolution issue is solved by using pseudo-inverse-based formulation and by considering different optimization criteria, such as maximizing the singularity-free workspace and improvising dexterity etc. However, it is found that the redundancy-resolution can be effectively achieved by using online optimization techniques.

In present work, the following objectives are planned:

(i) Consider a planar configuration and introduce kinematic redundancy

(ii) Arrive the kinematics and workspace characteristics in comparison to non-redundant case

(iii) Select the stiffness improvisation as the criterion and define isotropic stiffness index in terms of Jacobian matrix.

(iv) Choose a workpath inside the workspace of manipulator and divide it into several check points. At each point, the objective is to achieve isotropic stiffness index.

(v) To maximize the stiffness index, two non-conventional global optimization schemes are to be considered.

(vi) The identified optimized locations of redundant prismatic joints are to be tested with forward static analysis problem.

(vii) Create the optimized dimensions of redundant manipulator in ADAMS simulation environment and test the inverse solution.

(viii) Finally fabricate a prototype of assembly and propose the guidelines for its control.

The remaining part of thesis is organized as follows: chapter-2 explains the kinematics and definition of stiffness matrix of redundant parallel manipulator under consideration. Chapter-3 deals with the description of two latest meta-heuristic algorithms (new spiral optimization scheme and Particle swarm optimization) for solving the stiffness optimization of the manipulator. Results and discussion of the work are presented in chapter-4. In chapter-5, summary and future direction of the work is explained.

Chapter 2

Mathematical Modeling

2.1 The 3-RPR Manipulator Description

The base architecture on which the study is based is presented in Figure 2.1.

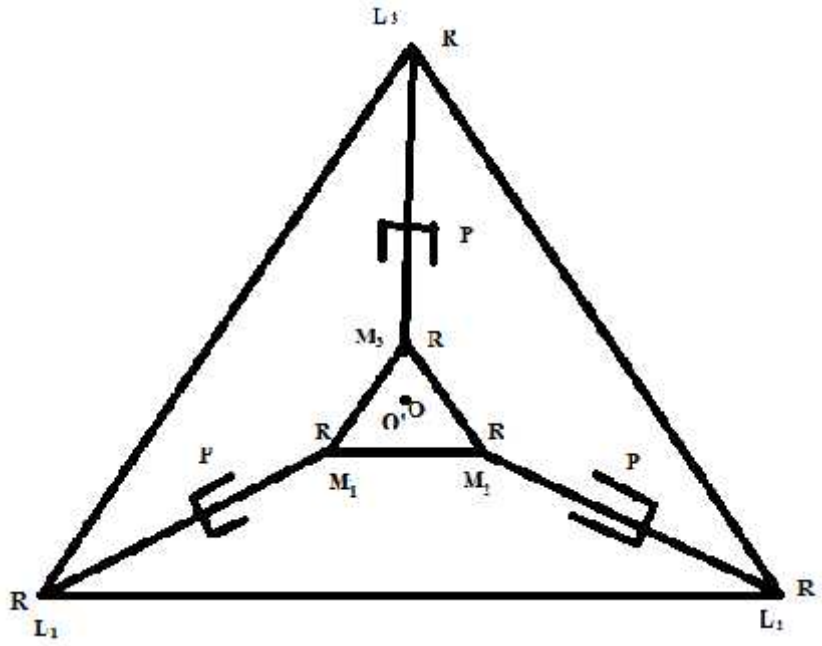

Fig. 2.1The 3-RPR Manipulator

It is a conventional and non-redundant type of manipulator. There are three limbs that connect the platform on the ground to the platform that moves, a point on which can be used as end effector. The former is labeled as $L_1L_2L_3$ and the latter as $M_1M_2M_3$. The vertices L_1 and M_1 are constrained through a leg with three joints. One of which is active and the other two are passive. The former is prismatic joint while the latter one is, revolute. The important feature of the manipulator is that it contains no complex singularity curves inside the workspace, unlike its popular 3-RRR counterpart. But, the

mechanical construction becomes heavy due to the inherent presence of a prismatic joint. The extension of any prismatic joint is t_{ij}, i.e. i^{th} limb and j^{th} joint.

2.2 Inverse Kinematics of 3-RPR Manipulator

In order to compute the velocities or displacements at limb joints for a desired trajectory of the end effector, inverse kinematics is necessary. There are two coordinate systems, shown in Fig 2.2. A fixed one which is on ground with the larger platform $L_1L_2L_3$. A mobile one that is attached to the end effector platform $M_1M_2M_3$. They are notated as O'-X-Y and O-x-y respectively.

A vector equation can be written for the system as follows:

$$\{O'M_i\}=\{O'O\}+[R]\{OM'_i\} \tag{2.1}$$

where [R] is the rotation matrix $\begin{bmatrix}\cos\phi & -\sin\phi \\ \sin\phi & \cos\phi\end{bmatrix}$, vector $O'O=\begin{Bmatrix}x\\y\end{Bmatrix}$ and $\{OM'_i\}$ is vector from O to M_i expressed in moving frame O-x-y.

Expanding the equation in matrix format,

$$\begin{bmatrix}M_{ix}\\ M_{iy}\end{bmatrix}=\begin{bmatrix}x\\ y\end{bmatrix}+\begin{bmatrix}\cos\alpha & -\sin\alpha\\ \sin\alpha & \cos\alpha\end{bmatrix}\bullet\begin{bmatrix}M'_{ix}\\ M'_{iy}\end{bmatrix} \tag{2.2}$$

2.3 Velocity Analysis of 3-RPR Manipulator

The time derivative of displacement results in velocity. The displacements of prismatic joints are t_{12}, t_{22} and t_{32}. The kinematic equations are written from the loop-closure equations and differential kinematics is written by taking first derivative of loop-closure equations. From kinematic equations, a mapping from end effector velocities in cartesian space to actuator velocities in joint space can be obtained, termed as the Jacobian. The

Jacobian matrix is the relation of small perturbation of input and the response of output. The distance formula is adapted to the coordinate system in Fig 2.2.

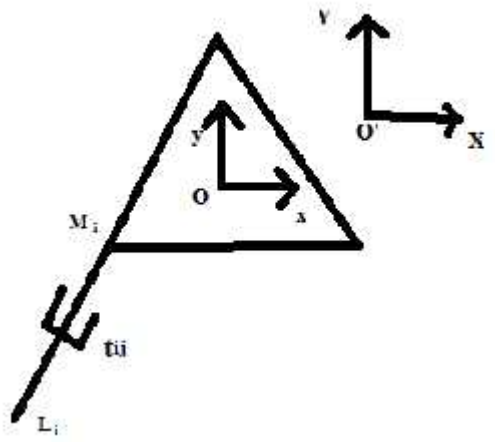

Fig. 2.2 Seperated Limb with Coordinate System

$$t_{i2}^2=(M_{xi}-L_{xi})^2+(M_{yi}-L_{yi})^2, \quad i=1,2,3 \tag{2.3}$$

where M_{xi} and M_{yi} are calculated from equation (2.1) and (2.2) as follows,

$$M_{xi}=x+(M'_{ix}\cos\phi-M'_{iy}\sin\phi) \text{ and } M_{yi}=y+(M'_{ix}\sin\phi-M'_{iy}\cos\phi) \tag{2.4}$$

Time-derivative of Eq.(2.3) yields:

$$2t_{i2}\dot{t}_{i2}=2(M_{xi}-L_{xi})\dot{M}_{xi}+2(M_{yi}-L_{yi})\dot{M}_{yi} \tag{2.5}$$

$$\dot{M}_{xi}=\dot{x}-(M'_{ix}\sin¤+M'_{iy}\cos¤)\dot{¤}=\dot{x}-OM_{yi}\dot{¤} \tag{2.6}$$

$$\dot{M}_{yi}=\dot{y}+(M'_{ix}\cos¤-M'_{iy}\sin¤)\dot{¤}=\dot{y}+OM_{xi}\dot{¤} \tag{2.7}$$

$$\hat{n}_{i2}=\frac{M_i-L_i}{t_{i2}} \tag{2.8}$$

And

$$\dot{t}_{i2} = (\dot{x} - (M'_{ix}\sin¤ + M'_{iy}\cos¤)\dot{¤})\hat{n}_{i2x} + (\dot{y} + (M'_{ix}\cos¤ - M'_{iy}\sin¤)\dot{¤})\hat{n}_{i2y} \tag{2.9}$$

Simplifying,

$$\dot{t}_{i2} = (\dot{x} - OM_{yi}\dot{¤})\hat{n}_{i2x} + (\dot{y} + OM_{xi}\dot{¤})\hat{n}_{i2y} \tag{2.10}$$

Expanding and Rearranging using matrix form,

$$\begin{bmatrix} \dot{t}_{12} \\ \dot{t}_{22} \\ \dot{t}_{32} \end{bmatrix} = \begin{bmatrix} \hat{n}_{12x} & \hat{n}_{12y} & OM_{x1}\hat{n}_{12y} - OM_{y1}\hat{n}_{12x} \\ \hat{n}_{22x} & \hat{n}_{22y} & OM_{x2}\hat{n}_{22y} - OM_{y2}\hat{n}_{22x} \\ \hat{n}_{32x} & \hat{n}_{32y} & OM_{x3}\hat{n}_{32y} - OM_{y3}\hat{n}_{32x} \end{bmatrix} \cdot \begin{bmatrix} \dot{x} \\ \dot{y} \\ \dot{¤} \end{bmatrix} \tag{2.11}$$

This is equivalent to,

$$A\dot{x} = B\dot{q} \tag{2.12}$$

That is the standard form of velocity equation for parallel manipulators. Comparing the two A and B matrices can be found and the Jacobian can be computed as,

$$J = B^{-1}A \tag{2.13}$$

2.4The 3-PRPR manipulator description

The mechanical architecture of the 3-PRPR parallel manipulator considered is shown in the Fig 2.3. It consists of a base platform, triangle $O_1O_2O_3$ and a mobile platform, triangle $M_1M_2M_3$. The end effector may be chosen as any suitable point on the mobile platform. The mobile platform is connected to the base platform through three parallel serial linkages called as limbs. Each limb consists of four joints, an actuated base prismatic joint along O_1L_1, a base revolute joint at L_1, an actuated distal prismatic joint along L_1M_1 and a platform revolute joint at M_1. Two prismatic joints are actuated. There are three limbs, hence twelve joints, but only six of them are actuated. The mechanism is

a planar one and has three degree of freedom. But the number of actuated joints is six. So three extra joints has to be actuated through a redundancy resolution algorithm.

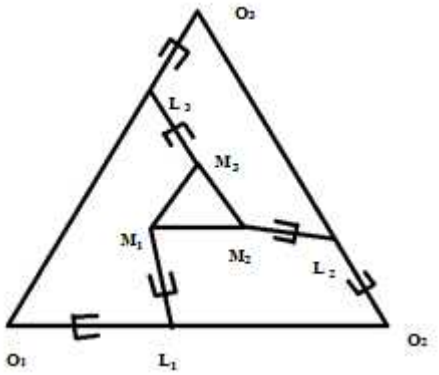

Fig. 2.3The 3-PRPR Manipulator

2.5 Kinematic and Jacobian Analysis of The 3-PRPR manipulator

The displacements of base prismatic joints are t_{11}, t_{21} and t_{31}. The displacements of distal prismatic joints are t_{12}, t_{22} and t_{32}. The velocity equations for the 3-PRPR mechanism can be obtained by modifying the kinematic equations of the 3-RPR to take into account the first time derivatives of base slider positions. Writing the displacement constraint from Fig. 2.4 in as equation 2.14.

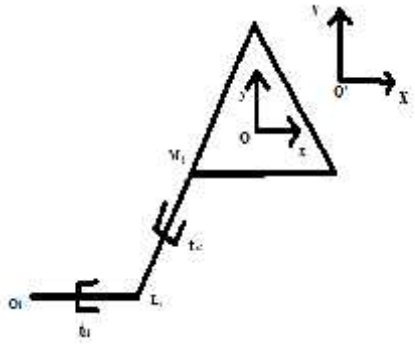

Fig. 2.4 Seperated limb of the 3-PRPR mechanism

$$t_{i2}^2 = (M_{xi} - L_{xi})^2 + (M_{yi} - L_{yi})^2, \quad i=1,2,3 \tag{2.14}$$

where, $\dot{M}_{xi} = \dot{x} - (M'_{ix}\sin¤ + M'_{iy}\cos¤)\dot{¤} = \dot{x} - OM_{yi}\dot{¤}$ (2.15)

$$\dot{M}_{yi} = \dot{y} + (M'_{ix}\cos¤ - M'_{iy}\sin¤)\dot{¤} = \dot{y} + OM_{xi}\dot{¤} \quad (2.16)$$

Writing the time derivative of equation (2.14) and not neglecting the base slider motion,

$$2t_{i2}\dot{t}_{i2} = 2(M_{xi} - L_{xi})(\dot{M}_{xi} - \dot{L}_{xi}) + 2(M_{yi} - L_{yi})(\dot{M}_{yi} - \dot{L}_{yi}) \quad (2.17)$$

$$\dot{t}_{i2} = (\dot{x} - (M'_{ix}\sin¤ + M'_{iy}\cos¤)\dot{¤} - \dot{t}_{i1}\hat{n}_{i1x})\hat{n}_{i2x} + (\dot{y} + (M'_{ix}\cos¤ - M'_{iy}\sin¤)\dot{¤} - \dot{t}_{i2}n_{i1y})\hat{n}_{i2y} \quad (2.18)$$

Where,

$$\hat{n}_{i1} = \frac{L_i - O_i}{t_{i1}} \quad (2.19)$$

$$\hat{n}_{i2} = \frac{M_i - L_i}{t_{i2}} \quad (2.20)$$

$$\dot{t}_{i2} = (\dot{x} - OM_{yi}\dot{¤} - \dot{t}_{i1}n_{i1x})\hat{n}_{i2x} + (\dot{y} + OM_{xi}\dot{¤} - \dot{t}_{i1}n_{i1y})\hat{n}_{i2y} \quad (2.21)$$

Expanding the equation 2.21 and rearranging in the matrix form,

$$\begin{bmatrix} n_{11}{}^T n_{12} & 1 & 0 & 0 & 0 & 0 \\ 0 & 0 & n_{11}{}^T n_{12} & 1 & 0 & 0 \\ 0 & 0 & 0 & 0 & n_{11}{}^T n_{12} & 1 \end{bmatrix} \begin{bmatrix} \dot{t}_{11} \\ \dot{t}_{12} \\ \dot{t}_{21} \\ \dot{t}_{22} \\ \dot{t}_{31} \\ \dot{t}_{32} \end{bmatrix} = \begin{bmatrix} \hat{n}_{12x} & \hat{n}_{12y} & OM_{x1}\hat{n}_{12y} - OM_{y1}\hat{n}_{12x} \\ \hat{n}_{22x} & \hat{n}_{22y} & OM_{x2}\hat{n}_{22y} - OM_{y2}\hat{n}_{22x} \\ \hat{n}_{32x} & \hat{n}_{32y} & OM_{x3}\hat{n}_{32y} - OM_{y3}\hat{n}_{32x} \end{bmatrix} \cdot \begin{bmatrix} \dot{x} \\ \dot{y} \\ \dot{¤} \end{bmatrix} \quad (2.22)$$

This is equivalent to,

$$A\dot{x} = B\dot{q} \quad (2.23)$$

That is the standard form of velocity equation for parallel manipulators. Comparing the two A and B matrices can be found and the jacobian can be computed as,

$$J = B^{-1}A \tag{2.24}$$

2.6 The 4-RPR Manipulator

In order to understand the advantages of kinematically redundant linkage against redundantly actuated mechanism, in present case, we also considered 4-RPR (one extra leg) redundantly actuated linkage. The mechanical architecture of the 4-RPR planar parallel manipulator is shown in the Fig 2.5. It consists of a base platform, $L_1L_2L_3L_4$ and a mobile platform, $M_1M_2M_3M_4$. The end effector may be chosen as any suitable point on the mobile platform. The mobile platform is connected to the base platform through four parallel serial linkages called as limbs. Each limb consists of three joints, a base revolute joint at L_1, an actuated distal prismatic joint along L_1M_1 and a platform revolute joint at M_1. The prismatic joint is actuated. There are four limbs, hence twelve joints, but only four of them are actuated. The mechanism is a planar one and has three degree of freedom. But the number of actuated joints is four. So the extra joint has to be actuated through a redundancy resolution algorithm.

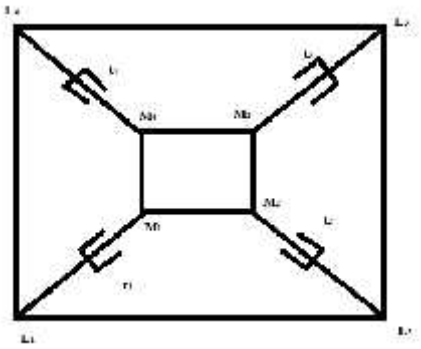

Fig. 2.5 The 4-RPR Manipulator

2.7 Kinematics and Jacobian Analysis of The 4-RPR Manipulator

The kinematics of the 4-RPR can be derived from the constraint equations of the four prismatic joints. The displacements of prismatic joints are t_1, t_2, $t_3$and t_4. The

displacements of distal prismatic joints are constrained within the minimum and maximum joint limits. The velocity equations for the 4-RPR mechanism can be obtained as follows, Writing the displacement constraint from Fig.2.6,

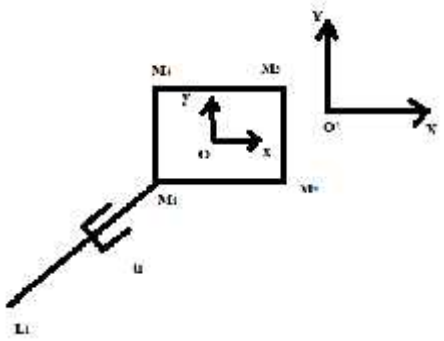

Fig. 2.6 Seperated limb of The 4-RPR mechanism

$$t^2{}_i = (M_{xi} - L_{xi})^2 + (M_{yi} - L_{yi})^2 \tag{2.25}$$

$$2t_i\dot{t}_i = 2(M_{xi} - L_{xi})\dot{M}_{xi} + 2(M_{yi} - L_{yi})\dot{M}_{yi} \tag{2.26}$$

Where,

$$\dot{M}_{xi} = \dot{x} - (M'_{ix}\sin¤ + M'_{iy}\cos¤)\dot{¤} = \dot{x} - OM_{yi}\dot{¤} \tag{2.27}$$

$$\dot{M}_{yi} = \dot{y} + (M'_{ix}\cos¤ - M'_{iy}\sin¤)\dot{¤} = \dot{y} + OM_{xi}\dot{¤} \tag{2.28}$$

Putting,

$$\hat{n}_i = \frac{M_i - L_i}{t_i} \tag{2.29}$$

$$\dot{t}_i = (\dot{x} - (M'_{ix}\sin¤ + M'_{iy}\cos¤)\dot{¤})\hat{n}_{ix} + (\dot{y} + (M'_{ix}\cos¤ - M'_{iy}\sin¤)\dot{¤})\hat{n}_{iy} \tag{2.30}$$

Simplifying,

$$\dot{t}_i = (\dot{x} - OM_{yi}\dot{¤})\hat{n}_{ix} + (\dot{y} + OM_{xi}\dot{¤})\hat{n}_{iy} \tag{2.31}$$

Expanding and writing in matrix form,

$$\begin{bmatrix} \dot{t}_1 \\ \dot{t}_2 \\ \dot{t}_3 \\ \dot{t}_4 \end{bmatrix} = \begin{bmatrix} \hat{n}_{1x} & \hat{n}_{1y} & OM_{x1}\hat{n}_{1y} - OM_{y1}\hat{n}_{1x} \\ \hat{n}_{2x} & \hat{n}_{2y} & OM_{x2}\hat{n}_{2y} - OM_{y2}\hat{n}_{2x} \\ \hat{n}_{3x} & \hat{n}_{3y} & OM_{x3}\hat{n}_{3y} - OM_{y3}\hat{n}_{3x} \\ \hat{n}_{4x} & \hat{n}_{4y} & OM_{x4}\hat{n}_{4y} - OM_{y4}\hat{n}_{4x} \end{bmatrix} \begin{bmatrix} \dot{x} \\ \dot{y} \\ \dot{\alpha} \end{bmatrix} \tag{2.32}$$

This is equivalent to,

$$A\dot{x} = B\dot{q} \tag{2.33}$$

That is the standard form of velocity equation for parallel manipulators. Comparing the two A and B matrices can be found and the jacobian can be computed as,

$$J = B^{-1}A \tag{2.34}$$

2.8 Generalized Stiffness Matrix

Several authors worked out on stiffness index as one of the measure of manipulator performance. A brief literature of few papers is cited below:

Simaan and Shoham [25] considered the stiffness synthesis of a kinematically redundant parallel robot. The proposed a polynomial solution for the geometric parameters in order to achieve a stiffness matrix. A six degree of freedom double planar parallel manipulator was studied and the polynomial obtained possessed 384 real solutions.

Legnani et al. [26] discussed isotropy and decoupling of n-dof parallel manipulators. The use of Jacobian matrix in achieving isotropy was revived. The application of these concepts to Gough-Stewart platform indicated that it can be isotropic, but not decoupled. A modification was proposed which resulted in two six degree of freedom isotropic and decoupled parallel manipulators.

Bandyopadhyay and Ghoshal [27] derived the Jacobian of Stewart platform that led an algebraic formulation in terms of an eigen value problem to obtain isotropy of the mechanism. The criterion for isotropy was expressed in terms of minimum number of

algebraic equations. Two families of manipulators with isotropic form were obtained using the symbolic algebraic equations.

Wu et al. [28] considered the effect of adding an additional leg to a 3-DOF parallel manipulator in terms of stiffness and natural frequency. The stiffness and natural frequency increased with the addition of a leg. But, addition of another leg was shown to be unnecessary. It was proposed to maintain symmetry of the mechanism in order to leave other kinematic paramters such dexterity unaffected.

A brief outline of stiffness prediction from kinematic equations is provided below:

Let $\dot{\theta}$ be the velocity of joint rates and $\dot{X}$ be the end effector velocity state,

Then, we have from jacobian analysis,

$$\dot{\theta} = J\,\dot{X} \tag{2.35}$$

For infinitesimal displacement

$$\partial\theta = J\partial x \tag{2.36}$$

This relates the infinitesimal joint displacement with the infinitesimal end efector displacement,

From duality between kinematics and dynamics,

$$F = J^T f \tag{2.37}$$

where F= End effector force vector

f = Joint Force Vector.

Stiffness is defined as force per unit displacement, hence joint forces can be defined as,

$$f = K_J \partial\theta \tag{2.38}$$

$$K_J = diag[K_1 .....K_n]$$

Hence,

$$F = J^T K_J J \partial x \tag{2.39}$$

Hence, The stiffness matrix is,

$$K = J^T K_J J \tag{2.40}$$

Here, K_t is a diagonal matrix containing stiffness of each actuator joint (known as rigidity coefficient). This stiffness is essential index in parallel manipulators for the following reasons:

(1) the higher stiffness can improve the dynamic accuracy.

(2) stiffness affects control performance.

To measure this matrix in different directions, the eigenvalues of stiffness matrix may be utilized. However, the units of the different entries of the matrix are not uniform, the dimensions of the eigenvalues of the stiffness include both force/length and force-length. Hence, the eigenvalue problem for stiffness is dimensionally inconsistent. Alternatively, the diagonal elements of stiffness matrix reflect pure stiffness.

Detailed expression for stiffness used in present work is given in next chapter.

Chapter 3

Optimization Techniques

This chapter presents a formulation of a present optimization criterion and two latest global optimization solution techniques via metaheuristics namely, spiral optimization and particle swarm optimization schemes.

3.1 Formulation of Optimization Problem

Optimization problem requires definition of objective function along with the constraints. Often both objective functions and constraints are nonlinear functions of a design variables. In the present work, we considered the redundant joint variables as the design parameters, so as to resolve the redundancy while satisfying the isotropic stiffness conditions over the workpath considered at the end effector.

Find the redundant joint locations so as to make the condition number of stiffness matrix S close to one. Here, S is defined as:

$$S = \frac{\min eigvalue([K])}{\max eigvalue([K])} \tag{3.1}$$

Where [K] is the stiffness matrix defined earlier in chapter 2,

Formulation is as follows,

At every checkpoint

Minimize |S-1|

Subject to: (the limits for the base prismatic actuators)

$$t_{i,\min} \le t \le t_{i,\max} \qquad (i=1, 2, 3) \tag{3.2}$$

We start from a selected workspace shape such as circle and square where the end-effector operates and at these locations, objective is to achieve isotropic stiffness index. The optimization procedure is as follows, at each checkpoint:

Step 1: Begin with a random set of feasible input candidate solutions.

Step 2: Define a series of checkpoints.

Step 3: Start with initial solution set.

Step 4: Compute Jacobian and hence, the Stiffness matrix at each checkpoint.

Step 5: compute the objective function and update the solution set based on selected meta-heuristics.

Step 6: Compare the updated vector set with the previous ones and store the potential candidates

Step 7: Repeat the procedure until optimal solution is found.

The discretization of the work region to a series of checkpoints, both on the boundary as well as on the inside reduce the computational requirements. The mechanism is useful if it is able to track any point within the desired workspace definitely while working against some load.

3.2 Spiral Optimization Methodology

Search algorithms are very often used for the purpose of solving optimization problems. Often many of the search algorithms are inspired from the phenomena in nature, e.g. bacteria foraging or birds flocking for food. Such higher order search principles are easy to implement, very robust and prone to convergence. The phenomenon that inspired this principle is present in various forms in nature such as in spirals generating logarithmically as in a shell.

Tamura and Yasuda [29,30] worked out a two dimensional spiral optimization algorithm and later proposed n-dimensional spiral optimization algorithm by extending the two dimensional algorithm. The n-dimensional rotation matrices were obtained as a composition of modified forms of 2-D rotation matrices. The algorithm was tested on different benchmark problems and the effectiveness of the algorithm was found to be competent as compared to other metaheuristics.

The method based on spiral optimization is quite suitable for higher dimensional problems. The spiral model begins by intiating randomly points representing solutions to a problem which converge iteratively to the centre of a spiral from the intial point. Each point in the progressive spiral is updated according to equation (3.3),

$$X^{k+1} = r.\, R_m\, X^k - (r.\, R_m - In)\, X^* \qquad (3.3)$$

Where,

X^{k+1} = Updated feasible solution

X^k = Previous feasible solution

R_m = The rotation matrix (here m refers to the number of design variables)

In = Identity matrix of order m×m.

r= radius of spiral (taken a value from 0 to 1)

Equation (3.4) gives the rotation matrix in the two dimensional space in terms of spiral angle ϕ:

$$R_2 = \begin{bmatrix} \cos¤ & -\sin¤ \\ \sin¤ & \cos¤ \end{bmatrix} \qquad (3.4)$$

In order to adopt the spiral optimization algorithm to n-dimensional problems, the concept of rotation in n-dimensions has to be formulated mathematically. One approach

to define the n-dimensional rotation matrices is to generalize the concept based on the two dimensional rotation matrices. The higher order matrices can be composed from the primary two dimensional rotation matrices with the help of eqn (3.5).

Rotations in m-dimensional Space is given by

$$R^m = \prod_{i=1}^{m-1} \left(\prod_{j=1}^{i} R^m_{n-i,m+1-j}(¤_{n-i,m+1-j}) \right) \tag{3.5}$$

For m=3, i.e. in three dimensional space,

$$R^3 = \prod_{i=1}^{3-1} \left(\prod_{j=1}^{i} R^n_{3-i,3+1-j}(¤_{3-i,3+1-j}) \right) \tag{3.6}$$

$$= \prod_{i=1}^{2} \left(\prod_{j=1}^{i} R^n_{3-i,4-j}(¤_{3-i,4-j}) \right)$$

$$\Rightarrow R^3 = R^3_{2,3}(¤_{2,3}) R^3_{1,2}(¤_{1,2}) R^3_{1,3}(¤_{1,3}) \tag{3.7}$$

The composition of the rotations can be obtained as follows,

$$R^m_{i,j}(¤_{i,j}) = \begin{bmatrix} 1 & & & & \\ & \ddots & & & \\ & & \cos¤_{i,j} & -\sin¤_{i,j} & \\ & & \sin¤_{i,j} & \cos¤_{i,j} & \\ & & & & \ddots \\ & & & & 1 \end{bmatrix}_{m \times m} \tag{3.8}$$

In 3 Dimensional Space, following sub-matrices are used to obtain R_m from eq.(3.5).

$$R_{1,2} = \begin{bmatrix} \cos¤ & -\sin¤ & 0 \\ \sin¤ & \cos¤ & 0 \\ 0 & 0 & 1 \end{bmatrix} \tag{3.9}$$

$$R_{2,3} = \begin{bmatrix} 1 & 0 & 0 \\ 0 & \cos¤ & -\sin¤ \\ 0 & \sin¤ & \cos¤ \end{bmatrix} \tag{3.10}$$

$$R_{1,3} = \begin{bmatrix} \cos¤ & 0 & -\sin¤ \\ 0 & 1 & 0 \\ \sin¤ & 0 & \cos¤ \end{bmatrix} \tag{3.11}$$

Flowchart of the algorithm is shown in Fig.3.1. The algorithm starts by initializing the parameters of spiral algorithm. Number of iterations has to be set by the analyst. The spiral angle and spiral radius are chosen based on experiments with the algorithm to obtain convergent results.

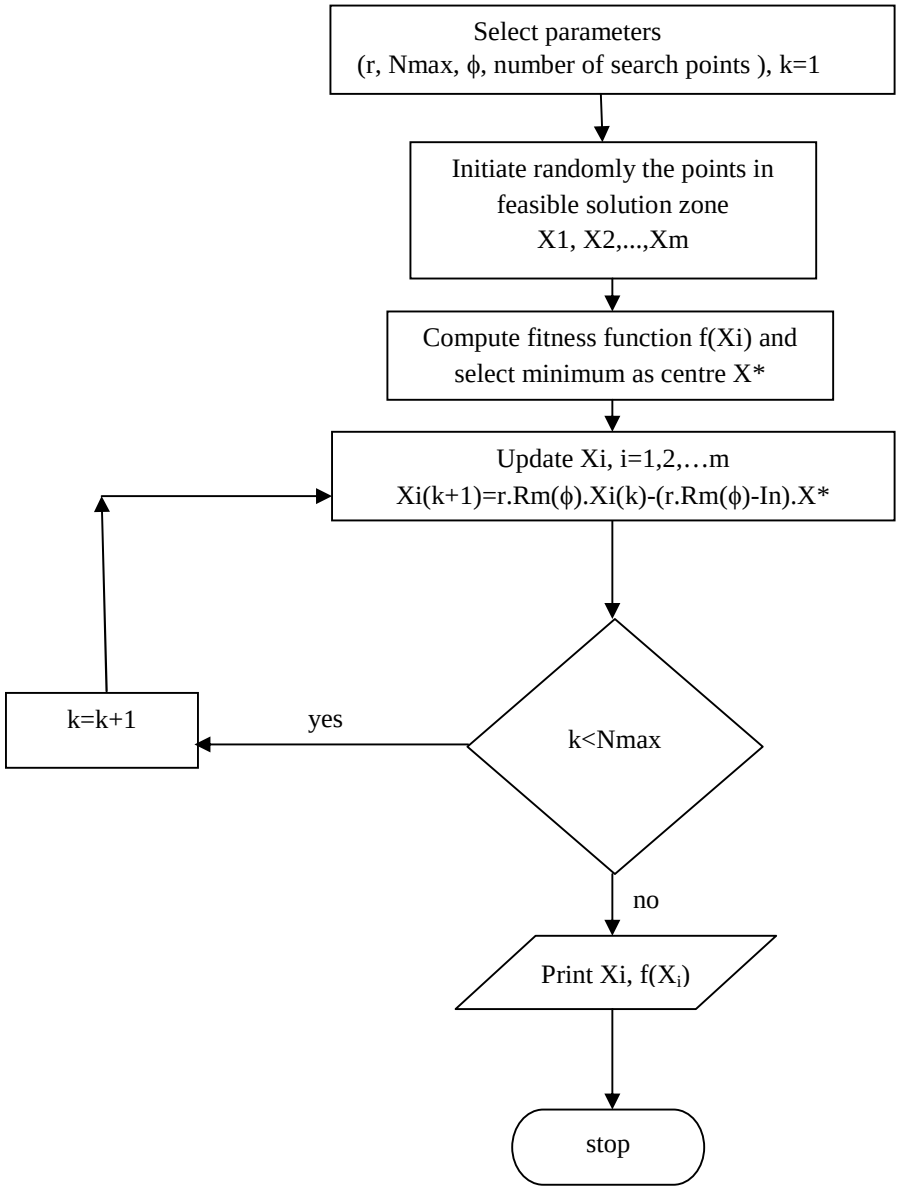

Fig.3.1 Flowchart of spiral optimization scheme

Some parameters suggested by Tamura and Yasuda [30] are shown in Table3.1. However, we have to carry-out trails to get correct set.

Table.3.1 Spiral Optimization Parameters

r (Spiral Radius)	¤ (Spiral Angle)
0.95	$\frac{®}{4}$
0.95	$\frac{®}{2}$
0.90	$\frac{®}{4}$

Next, a random set of vectors is generated within the feasible solution region. For each vector, the objective function is evaluated and the optimum solution is chosen as the starting point for a spiral with the parameters selected in the previous step. Each point is updated according to the equation (3.3). The centre of the spiral is chosen as the starting point of next iteration. After final iteration, the convergent solution is obtained and stored.

Here, k is the iteration number and Nmax is maximum number of iterations. A code has been written in MATLAB programming language. Any other programming language can also be used. The pseudo code with the procedure, parameters and formulae is provided here. The pseudocode is in line with the algorithm presented in flow chart in Fig.3.1.

Pseudo code:

%Initialize Parameters

¤ =pi/3; ; r=0.8;

Nmax=50; m=3;

In=eye(3);

%Generate Rotation Matrices

$$R_{1,2}=\begin{bmatrix}\cos¤ & -\sin¤ & 0\\ \sin¤ & \cos¤ & 0\\ 0 & 0 & 1\end{bmatrix};\quad R_{2,3}=\begin{bmatrix}1 & 0 & 0\\ 0 & \cos¤ & -\sin¤\\ 0 & \sin¤ & \cos¤\end{bmatrix};\quad R_{1,3}=\begin{bmatrix}\cos¤ & 0 & -\sin¤\\ 0 & 1 & 0\\ \sin¤ & 0 & \cos¤\end{bmatrix}$$

$$R_m = R_{12}R_{13}R_{23}$$

%Set Constraints

Xmin=[0;0;0];

Xmax=[X_1; X_2; X_3];

%Initial Variables Through Random Vectors

Loop

For 1:m

X_m= Xmin+rand(Xmax-Xmin);

End

Loop

For 1:Nmax

objf(m)=fitness(Xm);

X_{star}=max(objf);

%Constrain solution within limits

For k=1:m

$X^{k+1} = R_m X^k - (R_m - In) X_{star}$

if(X_m(k)>Xmax || X_m(k)<Xmin(k))

X_m(k)=Xmin+rand(Xmax-Xmin);

End

End

End

Print("%d, optimum value",X_{star})

The code was run on windows 7 platform in the Matlab environment on a machine with i-3 processor and 1 GHz speed. The novel algorithm is effective and gives convergent results for multidimensional problems.

3.3 Particle Swarm Optimization

This is one of the most popular optimization techniques. This has been inspired from the harmony in the flocking behavior of birds searching for food. This has been captured in the form of a dynamic principle. In this algorithm, a population of particles is spread over the feasible solution region. Then, each particle is updated based on the behavior of particles in its locality as well as particles in the generation. This is a dynamic process, one has to keep track of the best optimal values obtained by each particle and also, the

best value in the generation. A few such generations when iterated would lead towards a converging optimal solution.

Kennedy and Eberhart [31] presented the particle swarm optimization algorithm. The basic frame work of the algorithm based on flocking behavior of birds is simply based on three rules. First is to keep track of the speed of neighbourhood particles, second move towards the centre of the motion of the complete group and thirdly, not to jump out of bounds of solution.

The increment in the position of each particle is based on two factors as shown in Fig. 3.2.

1. Social weight
2. Personal weight

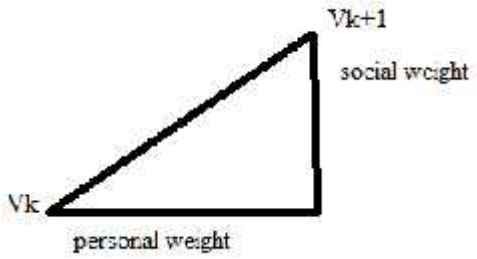

Fig 3.2 Particle Swarm

The conventional PSO approach is presented as a step-by-step method below:

(1) Define the initial swarm of populations, initialize the velocities and other constants.

(2) Evaluate fitness function for each particle of the swarm in each population.

(3) Store the personal best of each particle and obtain the global best of the population ‘Gbest’.

(4) If the new fitness value is better than the previous one , it becomes the new personal best and the new global best is obtained from the current values of each particle's personal best 'Pbest'.

(5) The new particle velocity is updated according to the following equation.

$$V_{k+1}=V_k+C_1r_1(Pbest-X_k)+ C_2r_2(Gbest-X_k) \quad (3.12)$$

Where, V_{k+1} = Updated particle velocity

V_k = Current Particle velocity

X_k= Current particle position

$C_1=C_2$=Social weight factors=2

$r_1=r_2$=randomly distributed value between 0 & 1.

(6) Update the particle position as follows,

$$X_{k+1}=X_k+V_{k+1} \quad (3.13)$$

Always one has to check the velocity and position upper and lower limits.

(7) After a number of iterations, a converging solution is obtained and the algorithm is stopped.

Selection of optimum parameters for particle swarm optimization is not a trivial task. But, in order to obtain global minima, proper selection of w, c_1 and c_2 is required. Li-ping et al. [32] presented criterion for selecting optimum parameters and Table 3.2 shows some suggested values.

Table. 3.2 PSO parameters

w	0.72984
c_1	2.05*w
c_2	2.05*w

Fig. 3.3 shows the flowchart of the algorithm to implement particle swarm optimization in the present work.

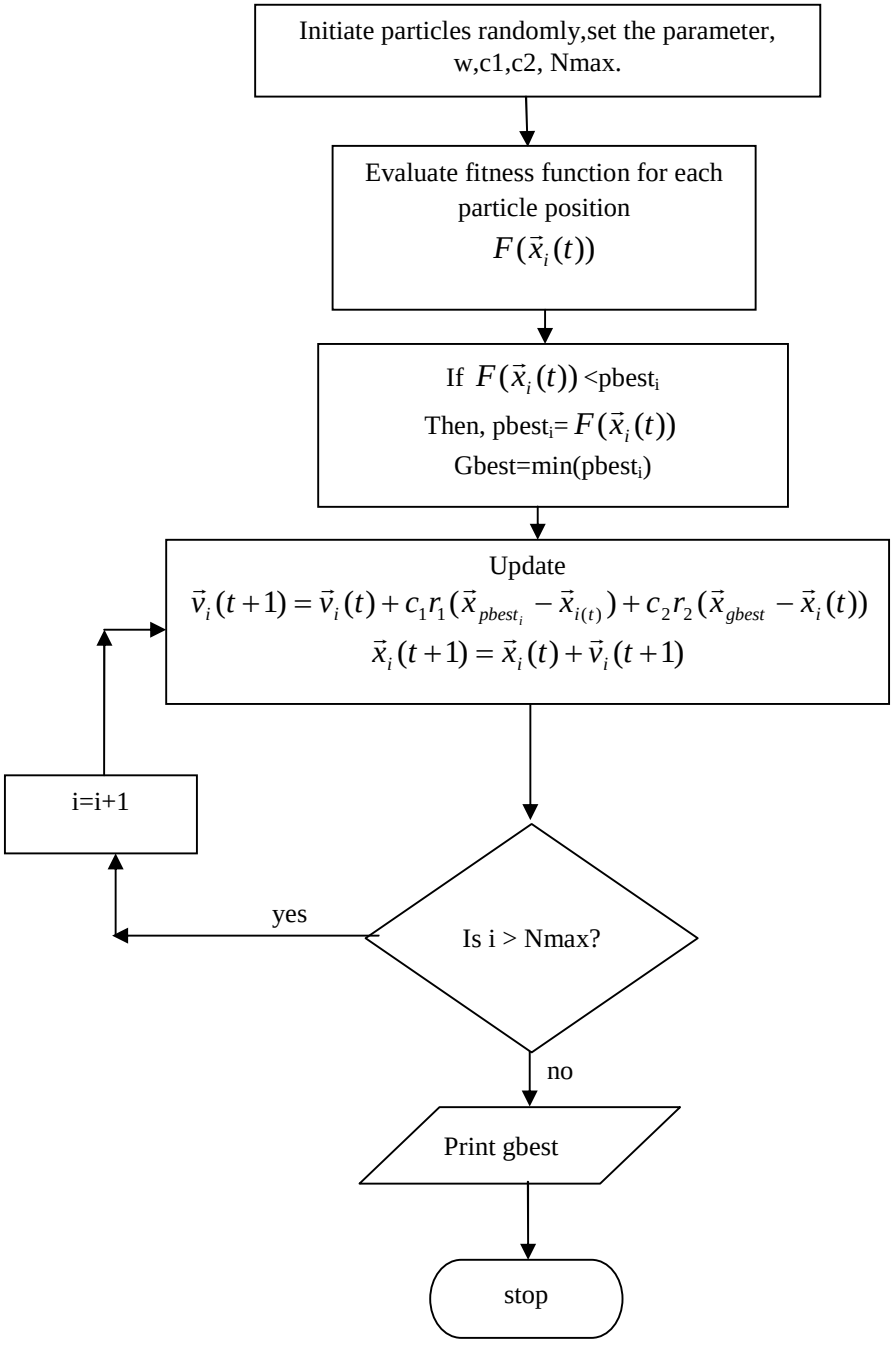

Fig 3.3 Flowchart for Particle Swarm Optimization

Similar to spiral optimization scheme, a simple program is developed in MATLAB for testing the present objective function. The code is initially tested for standard quadratic nonlinear objective functions. The parameters in this algorithm are higher than that in spiral optimization scheme.

Chapter 4

Results and Discussions

This chapter presents the simulation results relating to kinematics and optimization issues of non-redundant and redundant 3-RPR parallel manipulator.

4.1 Workspace and Singularity Analysis of 3-RPR manipulator

In order to illustrate the stiffness index optimization, we considered a working zone within the manipulator reachable workspace. In general, the workspace of the parallel manipulator consists of the set of points that can be reached by the end effector through a feasible configuration of its internal parts. There are many types of workspaces, namely dexterous workspace, reachable workspace, constant orientation workspace. The constant orientation workspace consists of the set of points reachable by the end effector at a fixed platform orientation. The reachable workspace consists of all points reachable by the end effector with at least one orientation. The dexterous workspace consists of the region spanned by the end effector with any orientation of the platform. Singularities occur when the configuration of the mechanism at a point in space becomes unstable. The mechanism either becomes locked up or some degrees of freedom are lost. At such points, the Jacobian of the mechanism becomes singular. Some singularity regions are grouped around the corners i.e. near workspace boundaries only. When manipulator works around the singular points or near singular regions, its accuracy, rigidity and other performances will become worse. In order to compute the workspace, a numeric discretization process is adopted. Table 4.1 shows the geometric parameters considered in

the kinematic analysis. To enhance workspace, often equilateral triangular platforms are considered. All the prismatic joints are having same range of sliding motion.

Table 4.1 Geometric Parameters of The 3-RPR

Base Platform Side	30 cm
Mobile platform Side	5 cm
Included Angle	60 degree
Joint Limits for Prismatic actuators (t_{min}, t_{max})	8 to 16 cm

Fig.4.1 and Fig.4.2 shows constant orientation workspace with singularity regions computed for the 3-RPR mechanism in two platform orientation of 30 and 60 degree angle respectively.

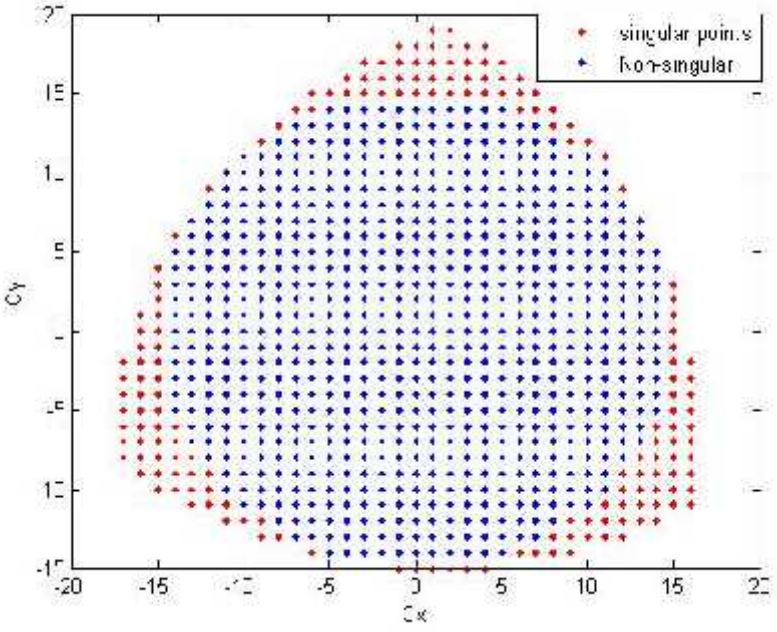

Fig.4.1 Workspace for Platform Orientation Angle, ¤ =30 degree

The singularities are present near the boundaries of the workspace only. So the complete central region is available for practical applications. But, still a significant amount of space is lost to singularities which can be recovered with the help of redundancies.

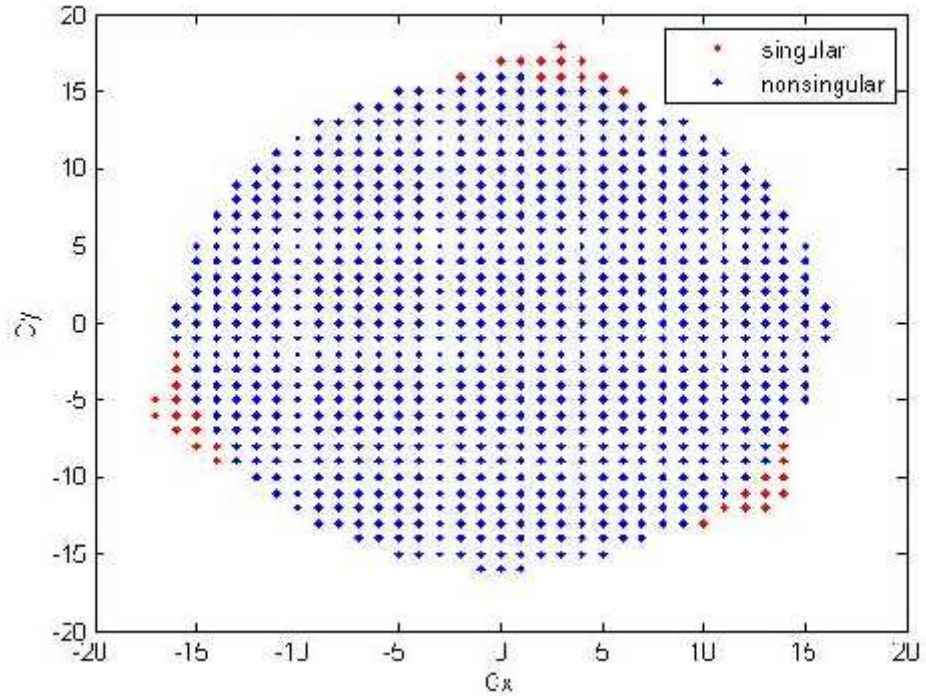

Fig. 4.2 Workspace for Platform Orientation Angle, ¤ = 60 degree

From Fig. 4.1 and Fig. 4.2, it is clear that the workspace for large orientation angle has maximal singularity free region. The workspace is limited due to the interference of the linkages. The singular region is reachable, but controllability of the actuation scheme is lost leading to unstable behaviour. Hence, there is a lot of scope to increase the usable workspace of the 3-RPR. Fig. 4.3 shows the workspace of 3-RPR embedded into the larger workspace of the 3-PRPR.

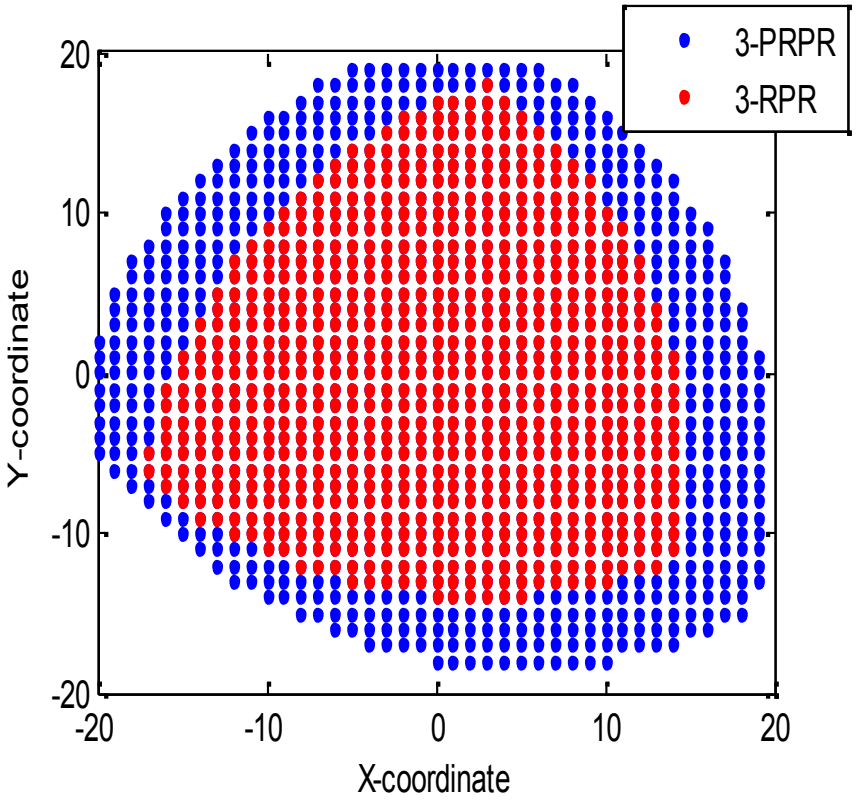

Fig. 4.3 The 3-PRPR reachable workspace

The 3-PRPR has no definite workspace shape, rather a variable workspace. But, it expands the workspace capability of the 3-RPR, by allowing singular configurations to become reachable via the internal reconfiguration of redundant parameters, thereby enhancing the workspace of the 3-RPR. Fig. 4.4 shows the workspace of 4-RPR actuation redundant manipulator containing the smaller workspace of 3-RPR. It represents another interesting case of redundancy which can be used to enhance capabilities such as workspace, stiffness etc of the non-redundant manipulator. Present work focuses on kinematically redundant manipulator analysis. So, workspace point of view

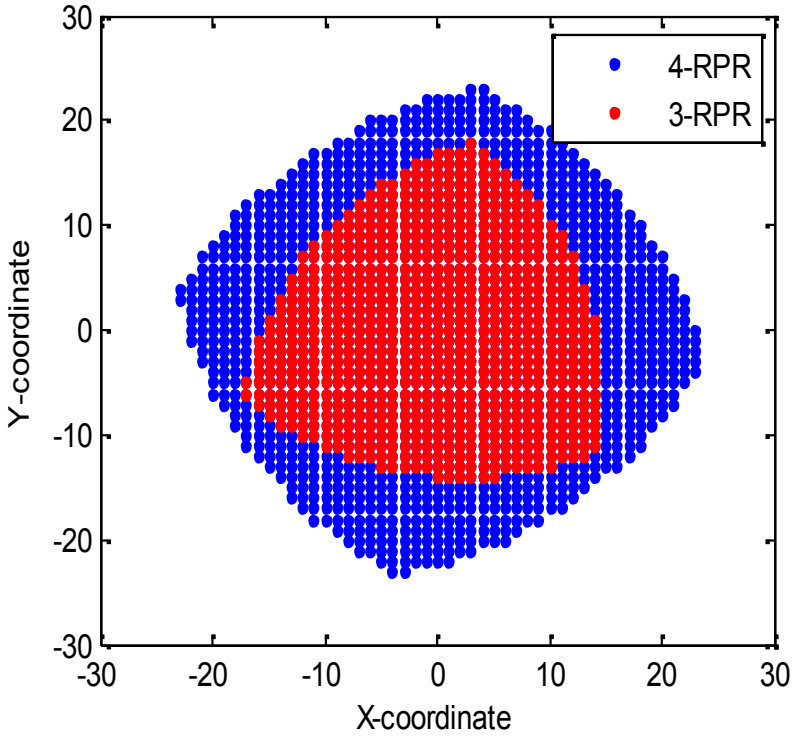

Fig.4.4 The 4-RPR workspace

4.2 Simulation Results using ADAMS software

Msc ADAMS is a commercial multibody dynamic analysis tool. It stands for automated dynamic analysis of mechanical systems. It allows to create the model of complete mechanical system including kinematic pairs and constraints. With the help of Msc ADAMS, a model of 3-RPR with geometric parameters in Table 4.1 was created as shown in Fig. 4.5. The base position of the model could be varied parametrically. An inverse kinematic simulation was run for a circular trajectory within the workspace and the feasibility of motion was tested. Since, there were no direct link intereferences, the solutions were feasible for the kinematic analysis of the mechanism.

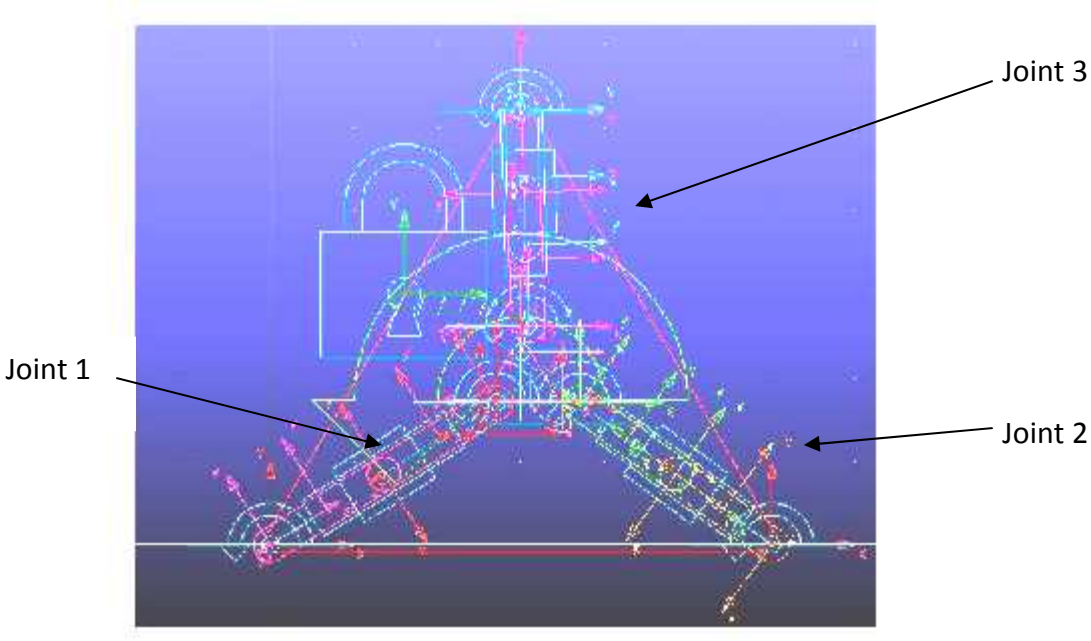

Fig. 4.5 Multibody Model of the 3-RPR Mechanism

A circular path was chosen with following equations for the end effector,

x=rcos(t), y=rsin(t);

where ,

x and y are the coordinates of the end effector

r is the radius of the trajectory. Specified 10 mm for current simulation of t=10 seconds.

The joint displacements as recorded during the inverse kinematic simulation are shown in Figures 4.6, 4.7 and 4.8. The active slider joint displacements are measured along the joint axes and displacements are found to be within the joint limits. In a similar way, we can obtain passive revolute joint angular displacements as a function of time.

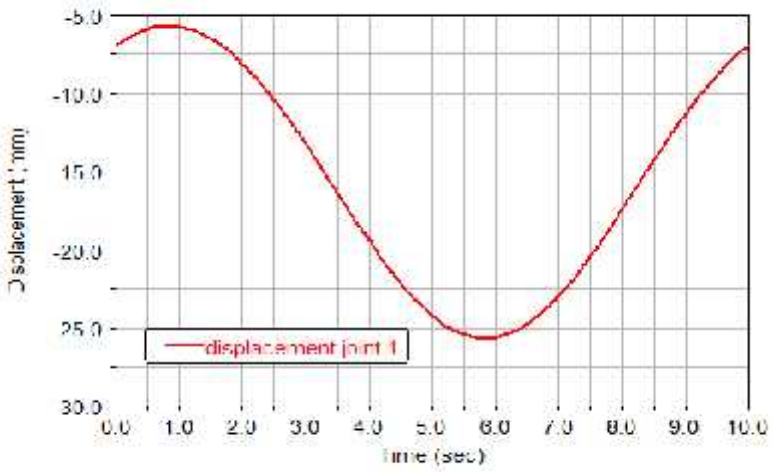

Fig. 4.6 Joint 1 Displacement vs Time

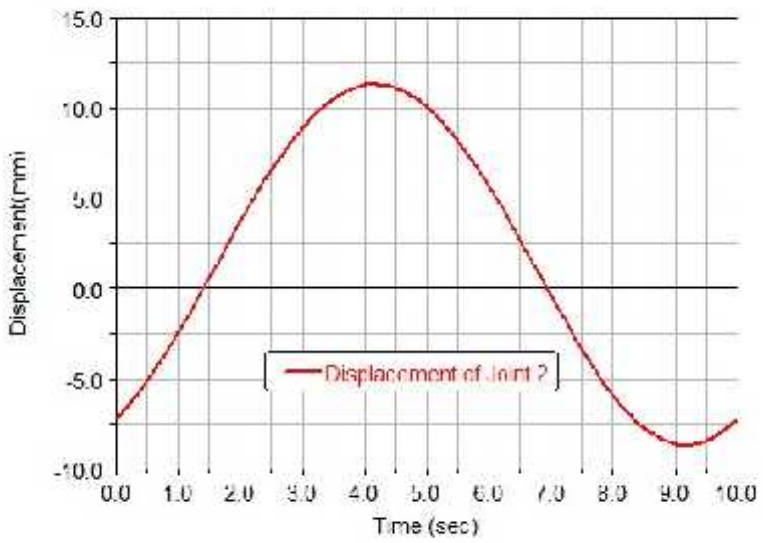

Fig. 4.7 Joint 2 displacement Vs time

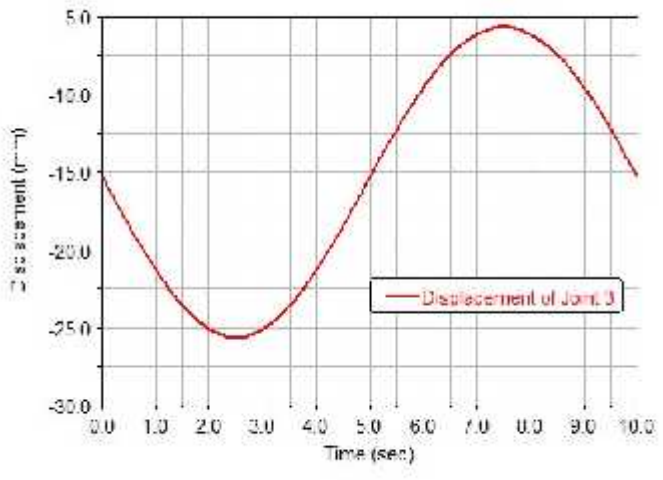

Fig. 4.8. Joint 3 displacement Vs time

The above inverse displacement solutions are verified with our code based on kinematic equations described earlier and it is found that an exact coincidence has occurred.

4.3 Stiffness Index Analysis and Optimization

The mechanism is useful if it is able to track any point within the desired workspace while working against some load. Since, for any useful work, the error due to deflection of the point tracing the required trajectory must be contained within limits. In case of redundancy obtained due to additional actuators in each limb of the manipulators, there exists infinite poses for achieving a target point within workspace. Hence, there is a need to resolve this difficulty. Further, the stiffness of mechanism is dependent on configuration of the mechanism; hence any strategy that takes into account stiffness as the driving factor will benefit the design procedure as a whole. Fig.4.9 shows an atlas of stiffness index for non-redundant 3-RPR linkage in a constant orientation pose. This is also developed with a Jacobian matrix formulation subroutine. It is seen that the stiffness

index at most of the locations especially at the central work region is relatively small and requires improvement.

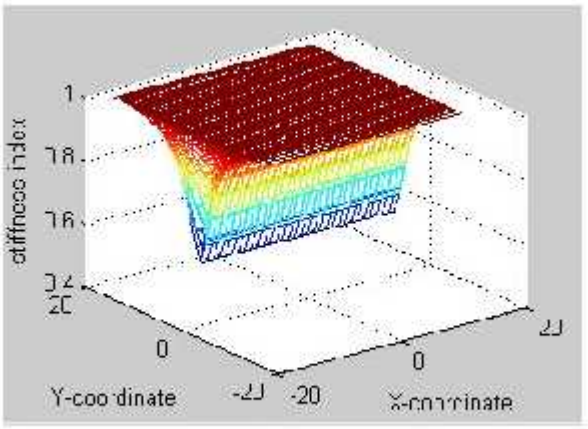

Fig.4.9 Atlas of stiffness index of 3-RPR mechanism

Envelop of usable workspace acts as a primary constraint and all the computations are performed on selected checkpoints within this space. It is seen that in manufacturing industry, many components are required to be fabricated on same machine. Majority of components consists of various features with standard shapes as circles, boundaries, triangle etc. In order to fabricate such components, the workspace of the device include should contain the desired feature boundary.

As a next case, 3-PRPR mechanism is considered with the specified range of redundant base slider actuator positions (0 to 5 cm). The maximum possible workspace with symmetrically laid base sliders is likewise computed as equivalent 3-RPR mechanism. Within the workspace, some region in the form of circular and square shapes is separately

considered as the working path of mechanism to present the optimization analysis. Objective is to achieve a maximum stiffness close to unity at the boundaries of these shapes and at interior choosen points. So the program employs Jacobian analysis at every Cartesian location of work shape compute the stiffness matrix and finally the stiffness index. This analysis involves nonlinear terms and requires some efficient optimization scheme.

Since, it is difficult and time taking to perform computation at each point within the workspace, certain selected points are used for the purpose of optimization. These points are referred to as checkpoints. Checkpoints may lie within or on the boundary of the workspace. The two workspaces under study are shown in Fig.4.10.

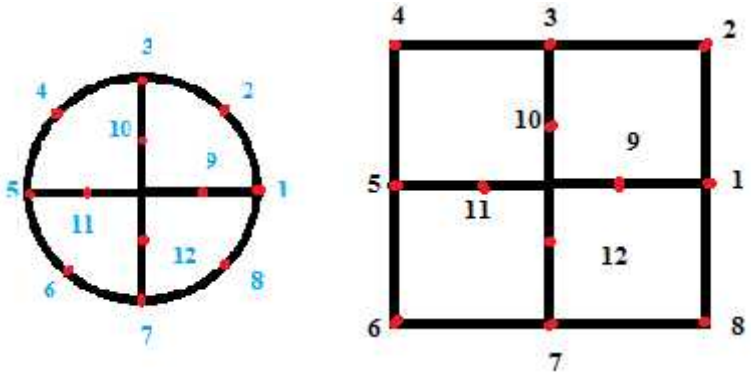

Fig.4.10 Workspaces with considered checkpoints

There are two work envelopes, a circular and a square. The checkpoints are marked on the boundary as well as on the inside. All points cannot be considered as it would form an exhaustive, but a very time consuming search and computational cost would go up. Hence, it is wise to discretize or mesh the workspace. Only, selected checkpoints need to be computationally verified for obtaining the optimal solution. First the optimization is conducted with spiral optimization scheme and then using particle swarm optimization.

The computer programs are developed for both these schemes in MATLAB environment and are verified with some standard problems. The constraints in the present formulation are the base joint lower and upper limits of displacements and velocities. The following parameters are employed (Tables 4.2 and 4.3) :

Table 4.2 Spiral Optimization algorithm parameters

r=0.8; a constant
Nmax=1000; maximum iterations
m=number of variables=3;
Spiral angle for rotation matrix is 60 degree.

The parameters used in PSO:

Table 4.3 Particle swarm algorithm parameters

nv=3;number of variables
popsize=50;size of population
Generations=1000;no. of generations
w = 0.72984; a constant
c1 = 2.05 * w;
c2 = 2.05 * w;

Case Study I:

A circular workspace is chosen first for the purpose of illustration. The workspace is discretized into twelve checkpoints: Eight checkpoints are on the boundary and four checkpoints lie inside the workspace. At each and every check point with specified (x,y)

coordinates, we require to find the Jacobian and stiffness at some pre-set values of base prismatic joint locations using simple 3-RPR kinematics. The convergence of the stiffness index is plotted against number of iteration cycles for first checkpoint as shown in Fig.4.11.

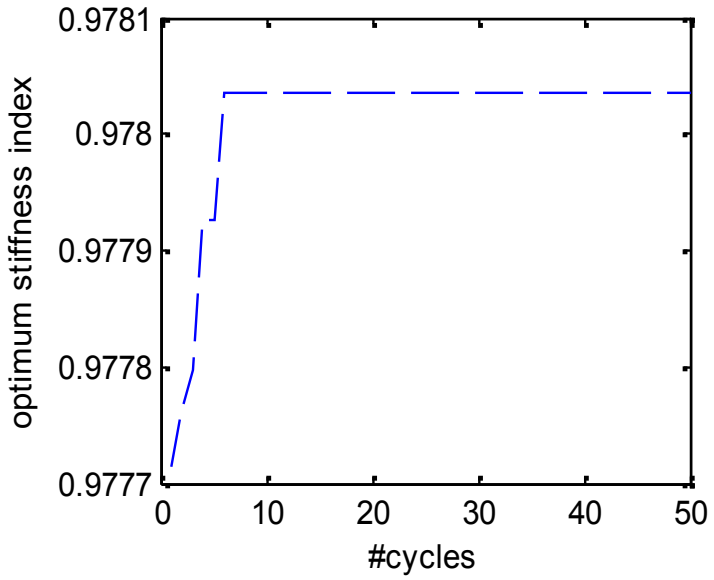

Fig. 4.11 Convergence of The Optimal Index at First Checkpoint

In order to test the validity of the obtained solution, one can test the mechanism for a set of joint forces, to see whether the output forces and moments are reasonable or not. A force of 10 Newton is applied at each distal actuator at fixed optimal base slider positions for each check point and the corresponding end-effector forces are computed through static analysis. Fig.4.11 shows the outputs. The values obtained are of reasonable levels.

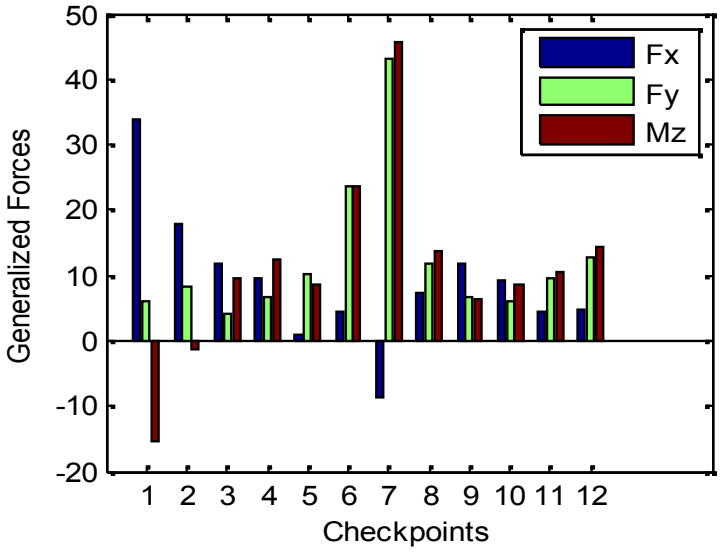

Fig. 4.12 Generalized End Effector Forces For a Test Input

(Input Force 10 Newton)

The effectiveness of the algorithm is compared with particle swarm optimization. Fig.4.13 shows, chart of optimal values of stiffness index obtained from particle swarm against spiral optimization. The spiral optimization is seen to be effective as the optimal values are much closer to unity.

Case Study II: Square Work region

A square work region with a given side length is considered. It is also divided into twelve checkpoints. There are eight on boundary and four on inside. The calculations are performed for the checkpoints on square workspace in the same way as done for the circular envelope earlier.

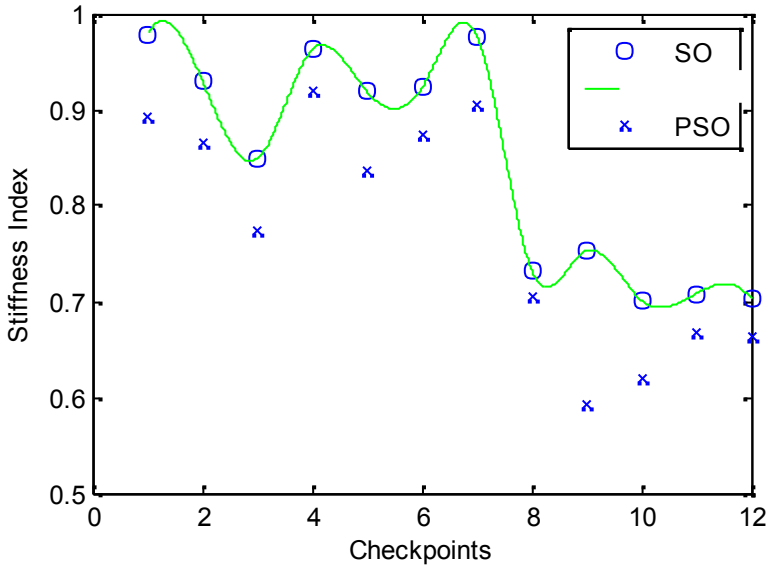

Fig. 4.13 Comparision between SO and PSO

After the first checkpoint, the procedure repeats on the subsequent points to perform the computations. One by one, all checkpoints shall be covered. An initial set of solutions is assumed for each case at the beginning. Then finally after a number of iterations, the procedure begins to give a convergent set and ultimate a solution is obtained. The convergence map is shown for one checkpoint as in Fig.4.14.

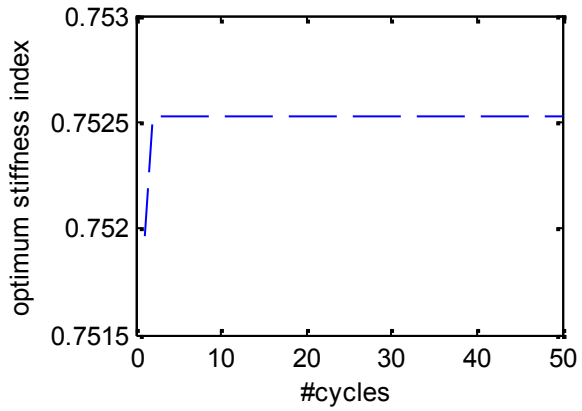

Fig. 4.14 Convergence for first checkpoint

Similar to circular case, a test the validity of the obtained solutions is performed by applying some input joint force and carry-out forward analysis to predict the end-effector forces. This is a mark of stiffness measure. Fig.4.15 shows the computed end-effector force vector at each point.

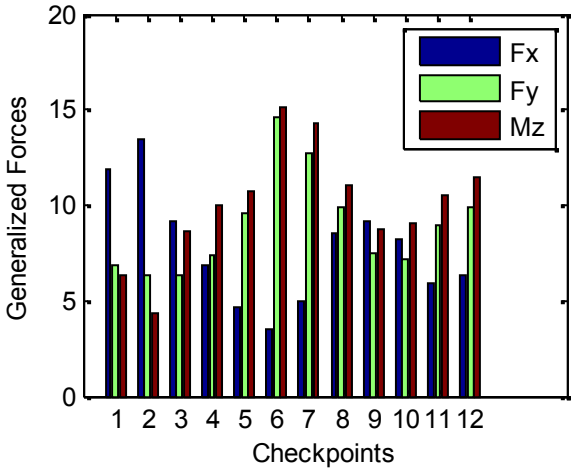

Fig. 4.15 General End Effector Forces (test input of 10 Newton)

Fig.4.16 shows the optimum stiffness index values obtained from PSO in comparison to spiral optimization scheme.

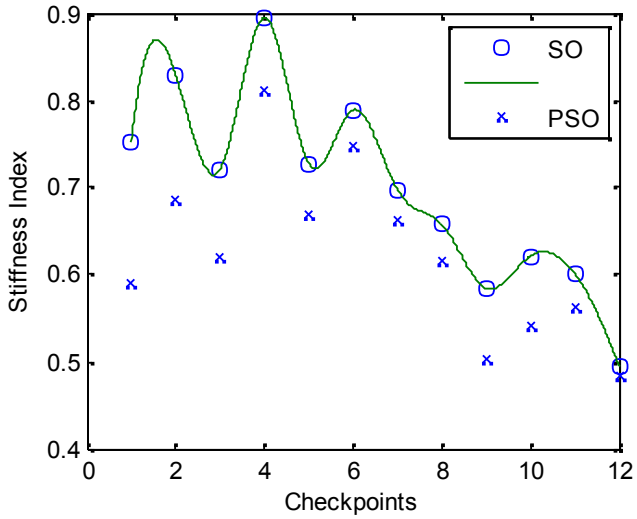

Fig. 4.16 Optimized stiffness indices at each check point

Novel spiral optimization scheme has given interesting results and corresponding optimized design variables are depicted for both cases in Table 4.4.

Table 4.4 Optimum design variables

Circular workshape				Square workshape			
Pt. No.	t_1 (m)	t_2 (m)	t_3(m)	Pt. No.	t_1 (m)	t_2 (m)	t_3(m)
1	3.09	4.98	0.06	1	2	4	0.65
2	4.99	4.98	4.95	2	0.56	4.98	3.25
3	0.05	3.23	4.98	3	0.05	2.55	3.22
4	1.11	0.23	4.96	4	1.11	0.23	4.96
5	1.99	4.01	0.06	5	4.98	4.83	4.76
6	2.12	3.02	4.5	6	4.99	1.56	3.12
7	3.08	3.33	4.89	7	0.02	2.09	1.43
8	1.50	2.33	4.66	8	4.99	4.89	0.06
9	4.30	4.40	4.85	9	1.39	4.99	3.90
10	4.08	0.91	2.97	10	0.09	2.92	1.97
11	4.84	4.98	4.90	11	4.11	4.98	4.99
12	3.09	4.98	0.06	12	2.52	4.98	1.56

4.4 Fabrication issues of scaled prototype

Within the limitations of time and resources, a simple manual set up for understanding of redundancies in 3-RPR linkage is developed using wooden and aluminum material at workshop. Initially, a solid model is drawn in Solidworks software and the feasibility is tested as done in ADAMS environment. The fabricated model shown in Fig.4.17 consists of the same 3-RPR mounted on variable base.

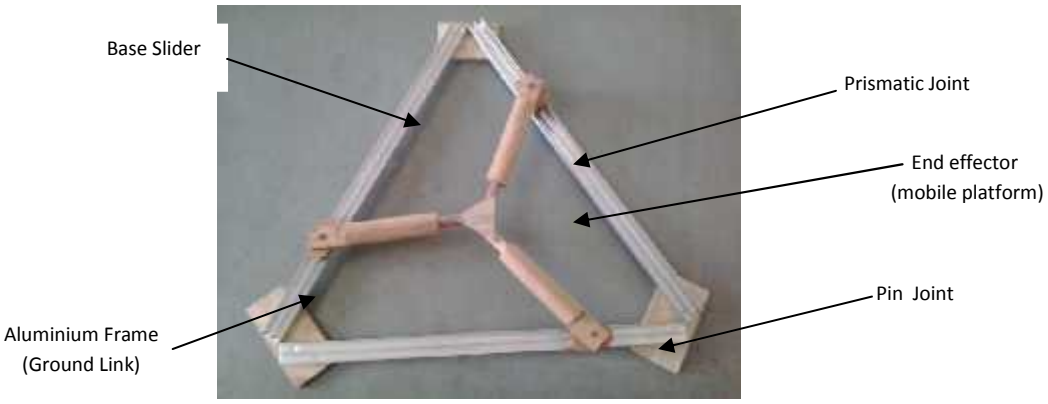

Fig. 4.17 Wooden skeleton model of the 3-PRPR

The model consists of a mobile platform, a fixed base and limb sub-assemblies. The mobile platform was carved out of a wooden plate as an equilateral triangle of 5 cm side length. Table 4.5 lists the dimensions.

Table 4.5 Parts and Materials

Component	**Material**	**Dimensions**
End Effector Plate	Timbre wood	5 cm
Base Platform	Aluminum Frame	30 cm
Limb Sub assembly	Timbre wood	10 cm (dead lenth) 20 cm (max extension)

The assembly consists of following parts:

1.Base platform: Base Platform, is fabricated from aluminum frame. There are two functions of the base platform. It serves as the ground link as well as accommodate the base slider joint. The mechanism intended to serve as a reconfigurable 3-PRPR planar parallel manipulator. Hence, the revolute joint of the limb sub assembly as shown in figure 4.18 should travel along the aluminium frame to allow changes in the position of the first passive revolute joint of the 3-RPR configuration resting on it.

2. Limb Sub assemblies: The limb sub assemblies were made out of wood. Dry timberwood is used for the fabrication. Each limb consist of three components, a base mount, a base cylinder and stepped rod. The base mount was fitted on to the aluminium frame with a slot to allow the relative base slider motion. The base cylinder has been pin jointed to the base mount at one end to permit relative rotational motion. The stepped wooden rod fits at one end into the base cylinder. The other end of the stepped rod is pin jointed to the end effector plate.

Fig. 4.18 Limb sub assembly

3. End effector: The end effector plate is carved out of timbre wood. It is an equilateral triangle with side length 5 cm. The end effector plate is connected to the three limb sub assemblies through pinned joints to permit relative rotational motions.

The workability of the mechanism is the next issue and it is planned to provide a reconfigurable end-effector (gripper) instead of rigid mobile platform. The trajectory tracking issues are yet to be verified with the use of linear motors in the assembly.

Chapter 5

Conclusion

In this work, the redundancy resolution for the 3-PRPR kinematically redundant parallel manipulator has been achieved using two optimization schemes namely: spiral and particle swarm optimizations to obtain the isotropic stiffness index inside a work region by proper selection of base slider positions. The optimum base slider positions has been obtained for the mechanism at selected checkpoints of a usable workshape defined within the maximum workspace of the kinematically redundant mechanism. Circular and square workshapes were considered, where twelve checkpoints distributed over the boundary and inner region of the workshape were selected in order to minimise the time and cost of computations while maintaining the accuracy of the results. The optimum base slider positions obtained by novel spiral otimization algorithm were closer to the desired objective function when compared against the particle swarm optimization technique. The workspace and singularity regions of 3-RPR linkage has been obtained and it is found that an enhancement can be obtained with the help of kinematic redundancy. The case of 4-RPR actuation redundant manipulator was briefly discussed and its workspace was analyzed. The solid model of the mechanism analysed in ADAMS software has given some interesting inverse kinematics outputs. After achieving optimal locations, forward kinematic analysis was carried out to verify the closeness of selected work shape and also the corresponding output forces were obtained from a given joint torques. A scaled model of the mechanism was fabricated and attempted to verify

the workspace features. In overall sense, the present study aids in the analysis and design of kinematically redundant manipulators effectively.

5.1 Future Scope

As future scope of this work, the 3-PRPR dimensions are to be arrived for any generalized work shapes with isotropic stiffness as criterion. An actual prototype with a computer controlled user interface is to be developed. The control system analysis and implementation for the manipulation is to be developed. A multiobjective formulation including other performance indices such as dexterity is to be set up. The dynamic analysis of the mechanism is an important task in the future. As an interesting case, a spatial form of 3-RPR manipulator with vertical prismatic bases can also be made up and the present algorithm can be verified for the spatial parallel manipulator in future.

APPENDIX

Listing of the function file for 3-PRPR

```
%%% FUNCTION TO COMPUTE OBJECTIVE (STIFFNESS INDEX)FOR THE OPTIMIZATION
%%% PROGRAMS.

function Z = aniket2(X3,x,y,phi)
l=5;
L=30;
prad=l/sqrt(3);
dmin=0;
dmax=30;

%Output in cartesian space
% phi=pi/3;
% x=2.5;
% y=2.5;

%redundant parameter
s1=X3(1);
s2=X3(2);
s3=X3(3);

%COOrdinates fOr platfOrm lOcatiOns in platfOrm cOOrdinate system

%cOOrdinates fOr O1
O1x= -(L/2);
O1y= -(L/(2*sqrt(3)));
%cOOrdinates fOr O2
O2x=  (L/2);
O2y= -(L/(2*sqrt(3)));
%cOOrdinates fOr O3
O3x=   0;
O3y=  (L/sqrt(3));

%cOOrdinates fOr first prismatic jOint parametrically defined

%cOOrdinates fOr A1
A1x= O1x+s1;
A1y= -(L/(2*sqrt(3)));
%cOOrdinates fOr A2
A2x=  O2x-s2*cos(pi/6);
A2y= O2y+s2*sin(pi/6);
%cOOrdinates fOr A3
A3x=   s3*sin(pi/6);
A3y=  -s3*cos(pi/6)+(L/sqrt(3));

%COOrdinates fOr platfOrm revOlute jOints in platfOrm cOOrdinate system

%cOOrdinates fOr B1
PB1x=(-l/2);
```

```
PB1y=(-l/(2*sqrt(3)));
%cOOrdinates fOr B2
PB2x=(l/2);
PB2y=(-l/(2*sqrt(3)));
%cOOrdinates fOr B3
PB3x=(0);
PB3y=(l/sqrt(3));

%cOOrdinates fOr platfOrm revOlute jOint in platfOrm cOOrdinate system

%platfOrm revOlute jOint B1
pb1x=PB1x*cos(phi)-PB1y*sin(phi);
pb1y=PB1x*sin(phi)+PB1y*cos(phi);
%platfOrm revOlute jOint B2
pb2x=PB2x*cos(phi)-PB2y*sin(phi);
pb2y=PB2x*sin(phi)+PB2y*cos(phi);
%platfOrm revOlute jOint B3
pb3x=PB3x*cos(phi)-PB3y*sin(phi);
pb3y=PB3x*sin(phi)+PB3y*cos(phi);

%cOOrdinates fOr platfOrm revOlute jOint in platfOrm cOOrdinate system

%platfOrm revOlute jOint B1
B1x=x+PB1x*cos(phi)-PB1y*sin(phi);
B1y=y+PB1x*sin(phi)+PB1y*cos(phi);
%platfOrm revOlute jOint B2
B2x=x+PB2x*cos(phi)-PB2y*sin(phi);
B2y=y+PB2x*sin(phi)+PB2y*cos(phi);
%platfOrm revOlute jOint B3
B3x=x+PB3x*cos(phi)-PB3y*sin(phi);
B3y=y+PB3x*sin(phi)+PB3y*cos(phi);

%lengths fOr first prismatic actuatOr

p11=sqrt((A1x-O1x)^2+(A1y-O1y)^2);
p21=sqrt((A2x-O2x)^2+(A2y-O2y)^2);
p31=sqrt((A3x-O3x)^2+(A3y-O3y)^2);

%lengths fOr secOnd prismatic actuatOr

p12=sqrt((B1x-A1x)^2+(B1y-A1y)^2);
p22=sqrt((B2x-A2x)^2+(B2y-A2y)^2);
p32=sqrt((B3x-A3x)^2+(B3y-A3y)^2);

%unit vectOr alOng base prismatic jOint

n11=(1/p11)*[(A1x-O1x) (A1y-O1y)];
n21=(1/p21)*[(A2x-O2x) (A2y-O2y)];
n31=(1/p31)*[(A3x-O3x) (A3y-O3y)];

%unit vectOr alOng prOximal prismatic jOint

n12=(1/p12)*[(B1x-A1x) (B1y-A1y)];
n22=(1/p22)*[(B2x-A2x) (B2y-A2y)];
```

```
n32=(1/p32)*[(B3x-A3x) (B3y-A3y)];

%A matrix normalized using platform radius

A=[ n12(1) n12(2) (n12(2)*pb1x-n12(1)*pb1y)/prad;
    n22(1) n22(2) (n22(2)*pb2x-n22(1)*pb2y)/prad;
    n32(1) n32(2) (n32(2)*pb3x-n32(1)*pb3y)/prad];

%B matrix

B=[ n11*n12' 1   0        0      0        0;
    0        0   n21*n22' 1      0        0;
    0        0   0        0      n31*n32' 1];

%Homogeneous Overall jacObian fOr 3-prpr kinematically redundant
manipulator

J=pinv(B)*A;
kj=1;
stiff=kj*J'*eye(6)*J;
cnd=cond(stiff);
% cnd=cond(J,2);
%joint torque calculation at each point.

Z=abs(1/cnd-1);

%%%%%%%%%%%%%%%%%%%%%%%%%%%%%%%%%%%%%%%%%%%%%%%%%%%%%%%%%%%%%%%%%%%%%%%%%%%
```

REFERENCES

1. S. Lee and S. Kim, “Kinematic analysis of generalized parallel manipulator systems”, Proc. 32nd conference on decision and control, San Antonio, Texas, 1993, vol.2, pp. 1097-1102.
2. J.P.Marlet, ‘Redundant Parallel Manipulators’, Lab Robotic Automation, Vol. 8, pp. 17-24, 1996.
3. F.Firmani and R.P.Podhorodeski, ‘Force-unconstrained poses for a redundantly-actuated planar parallel manipulator’, Mechanisms and Machine theory, vol. 39, pp.459-476, 2004.
4. S.B. Noklebya, R. Fisherb, R.P. Podhorodeskib and F. Firmania, ‘Force capabilities of redundantly-actuated parallel manipulators’, Mechanism and Machine Theory, vol.40, pp.578–599, 2005.
5. J.Wu, J.Wang, L.Wang and T.Li, ‘Dynamics and control of a planar 3-DOF parallel manipulator with actuation redundancy’, Mechanism and Machine Theory, vol.44, pp.835-849, 2010.
6. A.Muller and T.Hufnagel, ‘Model-based control of redundantly actuated parallel manipulators in redundant coordinates’, Robotics and Computer integrated Manufacturing, vol.60, pp.563-571, 2012.
7. H.Shin, S.Lee, J. I.Jeong and J.Kim, “Antagonistic stiffness optimization of rdundantly actuated parallel manipulators in a predefined workspace”, IEEE Trans. Mechatronics, vol.18, pp.1161-1168, 2013.

8. M G. Mohamed and C. Gosselin, “Design and analysis of kinematically redundant parallel manipulators with configurable platforms”, IEEE transactions on Robotics, vol. 21, no. 3, pp. 277-287, 2005.
9. J. Wang, C. Gosselin, “Kinematic analysis and design of kinematically redundant parallel mechanisms”, Journal of Mechanical Design, Trans.ASME, vol.126, pp. 109-118 , 2004.
10. I.Ebrahimi, “Kinematic redundancy in planar parallel manipulators”, Graduation Thesis, University of New Burnswick, 2004.
11. I. Ebrahimi, Juan A. Carretero and R. Boudreau, “3-PRRR redundant planar parallel manipulator: Inverse displacement, workspace and singularity analyses”, Mechanism and Machine Theory, vol. 42, pp.1007–1016, 2007.
12. I. Ebrahimi, J. Carretero and R. Boudraeau, “Actuation Scheme for a 6-DOF Kinematically Redundant Planar Parallel Manipulator”,Proc. of 12th IFToMM World Congress, Besanc¸on, vol.2,pp.1001-1009, 2007.
13. I. Ebrahimi, J. Carretero and R. Boudreau, “Kinematic analysis and path planning of a new kinematically redundant planar parallel manipulator”, Robotica, vol. 26, pp no. 405-413, 2008.
14. S.H.Cha, T.A.Lasky and S.A.Velinsky, “Kinematically-redundant variations of the 3-RRR mechanism and local optimization-based singularity avoidance”. J Mechanics Based Design of Structures and Machines, vol.35, pp. 15–38, 2007.
15. S.H.Cha, T.A.Lasky and S.A.Velinsky, “Determination of the kinematically redundant active prismatic joint variable ranges of a planar parallel mechanism

for singularity-free trajectories", Mechanisms and Mach Theory, pp. 1032–1044, 2009.

16. G. Chen, H. Wang, Y. Zhao and Z. Lin ,"A kind of kinematically redundant planar parallel manipulator for optimal output accuracy", Proc. Mechanisms and Robotics Conferences,vol.7,pp no. 475-483, 2009.
17. J. Kotlarski, H. Abdellatif, T. Ortmaier and B. Heimann, "Enlarging the useable workspace of planar parallel robots using mechanisms of variable geometry", Proc. Reconfigurable Mechanisms and Robots, pp no.63-72, 2009.
18. J. Kotlarski, T. Thanh, B. Heimann and T. Ortmaier, "Optimization strategies for additional actuators of kinematically redundant parallel kinematic machines", proc. of International Conference on Robotics and Automation,vol. 1, pp no. 657-661, 2010.
19. S.Zarkandi, "Singularity analysis of a 3-PRRR kinematically redundant planar parallel manipulator", Journal of Mechanical Engineering vol. 41, pp. 1-6, 2010.
20. L.Weihmann, D.Martins and L.S.Coelho, "Force capabilities of kinematically redundant planar parallel manipulators." Proc. of the 13th World Congress in Mechanism and Machine Science; pp. 19-25, 2011.
21. M. Ruggiu and J. Carretero "Kinematic analysis of the 3-PRPR redundant planar parallel manipulator" Prof. of International Conference on Robotics and Automation, vol.2, pp. no. 540-541., 2011.
22. A.Gallant, R. Boudreau, M.Gallant, "Geometric determination of the dexterous workspace of n-RRRR and n-RRPR manipulators", Journal of Mechanism and Machine Theory, vol. 51, pp no. 159–171, 2012.

23. T. Thanh, J. Kotlarski, B. Heimann and T. Ortmaier,“Dynamics identification of kinematically redundant parallel robots using the direct search method”, Journal of Mechanism and Machine Theory, vol. 55, pp no. 104-121, 2012.

24. R. Boudreau, S. Nokleby, “Force optimization of kinematically-redundant planar parallel manipulators following a desired trajectory”, Mechanism and Machine Theory, vol.56, pp.138–155, 2012.

25. N. Simaan and M. Shoham, “Stiffness synthesis of a variable geometry six-degrees-of-freedom double planar parallel robot”, The International Journal of Robotics Research, Vol. 22, pp. 757-775, 2003.

26. G. Legnani, I. Fassi, H. Giberti, S. Cinquemani and D. Tossi, “A new isotropic and decoupled 6-DoF parallel manipulator”, Journal of Mechanisms and Machine Theory, Vol. 58, pp no. 64-81, 2012.

27. S. Bandyopadhyay and A. Ghoshal,“An algebraic formulation of kinematic isotropy and design of isotropic 6-6 Stewart platform manipulators”, Journal of Mechanisms and Machine Theory, Vol. 43, pp. no. 591-616, 2008.

28. J. Wu, T. Li, J. Wang and L. Wang,” Stiffness and natural frequency of a 3-DOF parallel manipulator with consideration of additional leg candidates”, Journal of Robotics and Autonomous Systems, Vol. 61, pp no. 868-875, 2013.

29. K. Tamura and K. Yasuda,”Spiral dynamics inspired optimization”, Journal of Advanced Computational Intelligence and Intelligent Informatics, Vol. 15, pp no. 1116-1122, 2011.

30. K. Tamura and K. Yasuda,"Primary study of spiral dynamics inspired optimization", IEEE transactions on electrical and electronic engineering, Vol.6, pp. 98-100, 2011.
31. J. Kennedy and R. C. Eberhart,"Particle swarm optimization", Proc. Of IEEE International Conference on Neural Network, Piscataway, pp.1942-48, 1995.
32. Z. Li-ping, Y. Huan-jun and H. Shang-xu,"Optimal choice of parameters for particle swarm optimization", Journal of Zhejiang University Science, Vol. 6, pp no.528-234, 2005.